Stochastic nucleosome disassembly mediated by remodelers and histone fragmentation

Xiangting Li[1, a)] and Tom Chou[1, 2, b)]

[1)]*Department of Computational Medicine, University of California, Los Angeles, CA 90095-1766 USA*

[2)]*Department of Mathematics, University of California, Los Angeles, CA 90095-1555 USA*

We construct and analyze monomeric and multimeric models of the stochastic disassembly of a single nucleosome. Our monomeric model predicts the time needed for a number of histone-DNA contacts to spontaneously break, leading to dissociation of a non-fragmented histone from DNA. The dissociation process can be facilitated by DNA binding proteins or processing molecular motors that compete with histones for histone-DNA contact sites. Eigenvalue analysis of the corresponding master equation allows us to evaluate histone detachment times under both spontaneous detachment and protein-facilitated processes. We find that competitive DNA binding of remodeling proteins can significantly reduce the typical detachment time but only if these remodelers have DNA-binding affinities comparable to those of histone-DNA contact sites. In the presence of processive motors, the histone detachment rate is shown to be proportional to the product of the histone single-bond dissociation constant and the speed of motor protein procession. Our simple intact-histone model is then extended to allow for multimeric nucleosome kinetics that reveal additional pathways of disassembly. In addition to a dependence of complete disassembly times on subunit-DNA contact energies, we show how histone subunit concentrations in bulk solution can mediate the disassembly process by rescuing partially disassembled nucleosomes. Moreover, our kinetic model predicts that remodeler binding can also bias certain pathways of nucleosome disassembly, with higher remodeler binding rates favoring intact-histone detachment.

I. INTRODUCTION

In eukaryotic cells, 147 base pairs of DNA wrap around each histone octamer. DNA binds to the histone octamer at approximately 14 sites to form a nucleosome core particle. Nucleosomes, in turn, help compact meters of DNA inside the nucleus[1,2], protecting DNA from other proteins and unwanted enzymatic activity[3,4]. On occasion however, nucleosomes have to partially or completely release the substrate DNA to allow access by DNA-processing enzymes. Histones thus have to simultaneously perform two contradictory functions[3]. While there is consensus that histone modification and chromatin remodeling are critical in epigenetic regulation[5], the details of how nucleosomes dynamically perform different tasks are not yet fully understood[6]. Therefore, it is essential to first understand the molecular mechanics and dynamics of histone-DNA interactions.

DNA at both nucleosome ends is transiently accessible due to spontaneous bond breaking. This nucleosome "breathing" has been identified using single-molecular biophysics techniques[7-10]. Based on these observations, a rigid base-pair nucleosome Markov model was proposed and computationally explored to characterize the mechanical response to external tensions[10-12], sequence dependence and positioning of nucleosomes[13,14], and salt dependence[15]. Recently, similar discrete stochastic binding and unbinding models have been used to describe target search by pioneer transcription factors[16-19].

In molecular dynamics studies, coarse-grain models and even all-atom molecular models of nucleosome unraveling have also been discussed recently, characterizing the free energy landscapes of nucleosomes and capturing the finer details during the process of unwrapping[20-23]. Despite these mechanistic studies and modeling efforts, quantification of histone unwrapping using the above approaches is computationally expensive. In particular, these simulation approaches make it difficult to study:

(i) rare but decisive events such as complete spontaneous unwrapping; and

(ii) indirect interactions with other DNA binding proteins via transient nucleosome breathing.

Thus, simple analytic descriptions of the dynamics of histone-DNA and nucleosome-protein interactions can provide a useful tool for estimating and efficiently testing molecular hypotheses of nucleosome-mediated chromatin remodeling. In this paper, we develop discrete stochastic Markov models that relate different elements of histone-DNA interactions to overall rates of nucleosome disassembly.

In the next section, we formulate two classes of models, one in which histones remain as an intact single molecule, and another in which they are composed of three major subunits that can successively dissociate from DNA. The first abstraction describes DNA as linearly unspooling from a contiguous footprint defined by the histone particle and extends earlier work[24]. The state-space structure of this simple model is then nested to describe the state space of more molecularly realistic models of histone fragmentation. Finally, catalysis of nucleosome disassembly can be mediated by remodeling factors such as transcription factors[25,26]. We will also model such cofactor-facilitated histone removal by incorporating competitive

---

[a)]Electronic mail: xiangting.li@ucla.edu

[b)]Electronic mail: tomchou@ucla.edu

DNA-protein binding within each of these two classes (intact-histone and fragmenting histone) of models.

Our primary goal is to provide a quantitative characterization of the first passage time (FPT) from an initial configuration to a totally dissociated state. We aim to provide a closed form expression or numerical procedure for evaluating these timescales under specific biophysical conditions.

II. MATHEMATICAL MODELS AND RESULTS

The approach we will take for all of our following models is to analyze a discrete state Markov model describing the time-evolution of a probability vector $\mathbf{P}$ of molecular configurations which obeys $\partial_t \mathbf{P} = \tilde{\mathbf{W}} \mathbf{P}$, where $\tilde{\mathbf{W}}$ is a model-dependent transition matrix. The state space and the transition matrix $\tilde{\mathbf{W}}$ will be appropriately defined for each type of model, including variants that incorporate protein-catalyzed nucleosome disassembly. By analyzing the specific subsets of the state space and the eigenvalues of the associated transition matrices $\tilde{\mathbf{W}}$, we derive results that predict the distribution of configurations and the statistics of disassembly times.

The complete state space in our models, $\Omega \cup \Omega^*$, consists of the set of bound states Ω and the set of detached states Ω^*. In general, the transition matrix coupling all states is $\tilde{\mathbf{W}}$. However, since transitions into Ω^* from Ω are typically irreversible in our analyses, we can define $\tilde{\mathbf{W}}$ to operate on states within and out of Ω. Henceforth, we describe the eigenvalues of $\tilde{\mathbf{W}}$, $\{\tilde{\lambda}_j\}_{j \geq 0}$, in descending order of their real parts. The principal eigenvalue $\tilde{\lambda}_0$ of $\tilde{\mathbf{W}}$ will be that with the largest real part. When transitions to Ω^* are assumed to be irreversible, $\tilde{\mathbf{W}}$ defined on Ω represents a sub-matrix with all eigenvalues having negative real parts. Using this nomenclature, the inverse of the eigenvalues describes the timescales associated with the stochastic dynamics of sets of configurations (described by eigenvectors) within the state space. For example, $-1/\tilde{\lambda}_0$ is the slowest timescale of decay to Ω^* in the stochastic dynamics.

Quantities like $\tilde{\mathbf{W}}$ carry a physical dimension of rate (1/time). To make our mathematical analysis notationally simpler, we will normalize $\tilde{\mathbf{W}}$ by the fastest rate in the model to make it dimensionless. In the rest of the paper, the dimensionless transition matrix and its associated dimensionless eigenvalues are denoted $\mathbf{W}$ and λ_0, respectively. Other conventions for mathematical symbols and objects are summarized in Table IV.

A. Linear peeling, simple histone model

Here, we first consider the stochastic dynamics of how a single histone particle peels from the DNA wrapping it. This approach is similar to that taken in Kim et al.[25], but we track simultaneous peeling from both ends of the histone particle and assume uniform binding and

unbinding rates along the DNA substrate. Parameters and variables used in this model are listed in Table I.
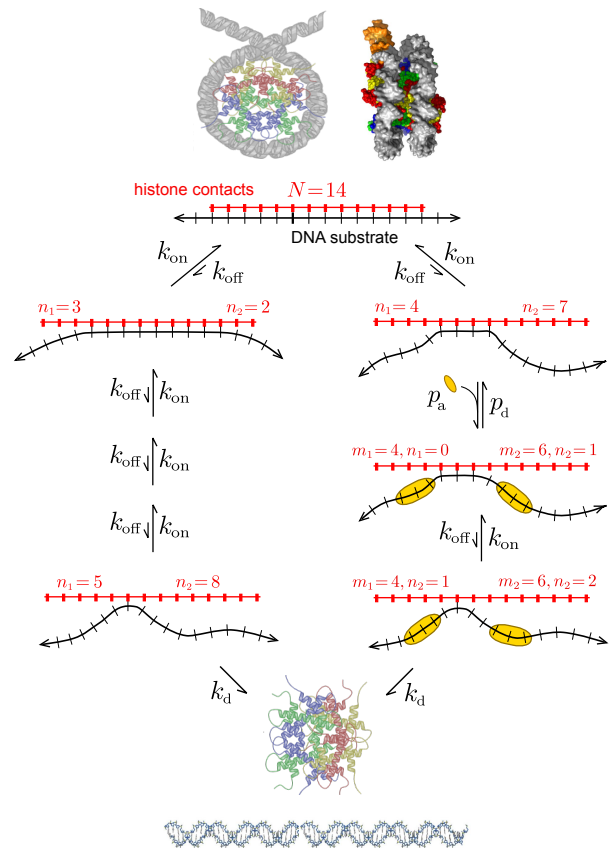
FIG. 1. A schematic of simple, intact-histone detachment. The unfacilitated and remodeler-facilitated pathways are shown on the left and right, respectively. Top image shows en face and sagittal views of a histone-DNA complex. Histone-DNA attachment points are described by discrete sites on a one-dimensional lattice. In this example, we illustrate $N = 14$ contact sites, evenly spaced by ~ 10 DNA base pairs, that each unbind and rebind with rates k_{off} and k_{on}, respectively. Protein or "remodelers" (yellow) can bind the DNA, occluding certain contacts sites and preventing them from rebinding DNA. Thus remodelers generate a ratchet mechanism accelerating nucleosome dissociation. In the remodeler-assisted model, m_1 and m_2 represent the number of cofactor-occluded contact sites on the left and right, respectively, and n_1, n_2 now represent the number of open contacts further to the right and left of m_1 and m_2, respectively. Detachment of the final contact occurs at rate k_{d}, which may be comparable to k_{off}.

1. Spontaneous histone-DNA detachment

Histone-DNA interactions typically consist of $N \approx 14$ possible contact sites. Each contact site on the DNA lattice may be in a bound (1) or unbound (0) configuration. If all contact sites are unbound at a specific time, the histone can be considered to be completely dissociated

parameter/variable	symbol	typical value
total number of DNA-histone contact sites	N	14
no. of open contacts right of the right-most protein-bound site on the right	n_1	–
no. of open contacts left of the left-most protein-bound site on the right	n_2	–
position of right-most protein-bound contact on the left	m_1	–
position left-most protein-bound contact on the right	m_2	–
DNA-histone contact site attachment rate	k_{on}	20-90s^{-1}
DNA-histone contact site detachment rate	k_{off}	$\sim 4\mathrm{s}^{-1}$
detachment rate of the final contact site	k_{d}	$\sim k_{\mathrm{off}}$
contact site binding free energy	$E_{\mathrm{c}} = \log(k_{\mathrm{off}}/k_{\mathrm{on}})$	-2
remodeler protein-DNA binding rate	p_{a}	–
remodeler protein-DNA unbinding rate	p_{d}	–
remodeler protein-DNA binding free energy	$E_{\mathrm{p}} = \log(p_{\mathrm{d}}/p_{\mathrm{a}})$	–

TABLE I. Parameters and variables used in linear peeling, intact-histone models. The distances between the inner-most bound contact and the inner-most remodeler-bound sites on the left and right are defined as n_1 and n_2, respectively. The distances from the inner-most remodeler-bound sites to the left and right ends of the N-total length contact segment are denoted m_1 and m_2, respectively, as shown in Fig. 1. In all subsequent analyses, we will measure all energies in units of $k_{\mathrm{B}}T$. Since k_{on} is the fastest rate in this system, our models and analyses will typically be presented in dimensionless form with rates measured in units of k_{on} and dimensionless parameters $\varepsilon \equiv k_{\mathrm{off}}/k_{\mathrm{on}} \ll 1$ and $s = k_{\mathrm{d}}/k_{\mathrm{on}} \ll 1$.

from the DNA at that time. Due to steric constraints, unbinding of the contacts will be assumed to occur sequentially from either end, as depicted in Fig. 1. Thus, the only way an interior site can be open is if all sites to the left or right of it are in an unbound state. In other words, histones can be peeled off only from the ends of their contact footprint. Under this assumption, the full configuration space $\{0,1\}^N$ can be reduced to a bound-histone state space $\Omega = \{(n_1, n_2) : n_1 + n_2 < N\}$ and a detached state $\Omega^* = \{(n_1, n_2) : n_1 + n_2 = N\}$, where n_1 and n_2 denote the number of detached histone-DNA bonds at the two ends of the histone-DNA contact footprint. In order to characterize the timescale associated with complete disassembly, we assume that the histone leaves the system once all contacts break. This defines a FPT problem to an "absorbing" detached state Ω^*.

The state space and the transitions within it can be visualized by random walks along the points in the triangular array along the n_1 and n_2 axes shown in Fig. 2(a). The transitions are driven by spontaneous detachment and attachment of single histone-DNA bonds with possibly sequence- and position-dependent rates k_{off} and k_{on}, respectively. We allow the dissociation rate k_{d} of the final contact to be different from k_{off}, since no other DNA-histone contact holds the histone in place. We expect this final-contact detachment rate to have magnitude $k_{\mathrm{d}} \sim k_{\mathrm{off}}$. In bulk genomic DNA, most sequences have similar binding energies with the histone octamer[27,28]. Thus, we first assume homogeneity in histone-DNA contact site binding energies and uniform association and dissociation rates k_{on} and k_{off}.

We define a dimensionless transition matrix by dividing the master equation by k_{on}, which we assume to be the fastest kinetic rate in our model. As detailed in Appendix A1, the dimensionless transition matrix $\mathbf{W} = \tilde{\mathbf{W}}/k_{\mathrm{on}}$ can be further decomposed as

$$\mathbf{W}(s) := \mathbf{A} + \varepsilon\mathbf{B} + s\mathbf{C}, \qquad (1)$$
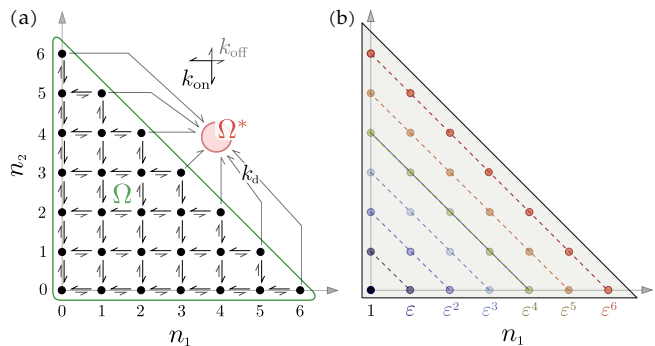
FIG. 2. (a) Schematic of a hypothetical attached-histone state space Ω for $N = 7$ (seven contact sites). Since there are $N(N+1)/2 = 28$ bound states, the transition matrix $\tilde{\mathbf{W}}$ is 28×28. Histone-DNA contacts increase and decrease by one with rate k_{on} and k_{off}, respectively, except the last contact which breaks with rate k_{d}. The completely detached absorbing state is indicated by Ω^*. (b) For a strongly binding system confined to Ω, $\varepsilon \equiv k_{\mathrm{off}}/k_{\mathrm{on}} \ll 1$, and a quasi-steady state distribution arises in which state probabilities $\sim \varepsilon^{n_1+n_2}$. The most probable states are those with small $n_1 + n_2$, corresponding to a tightly wrapped histone.

where $\mathbf{A}$ represents the transitions in which one extra bond is formed ($n_1 + n_2$ decreases by one), $\mathbf{B}$ describes the transitions of one bond being broken without leading to the detached state, and $\mathbf{C}$ indicates the transitions involving the breaking of the last contact, leading to the detached state. Matrices involving detachment, $\mathbf{B}$ and $\mathbf{C}$, are multiplied by the Boltzmann factor $\varepsilon \equiv k_{\mathrm{off}}/k_{\mathrm{on}} \equiv e^{E_{\mathrm{c}}}$ and $s \equiv k_{\mathrm{d}}/k_{\mathrm{on}}$, respectively. Here, E_{c} represents the change in free energy of forming contact site bond. For strong-binding contacts, $E_{\mathrm{c}} \ll -1$, and $\varepsilon, s \ll 1$. Physicochemical considerations suggest $s \sim \varepsilon$, but in our subsequent analysis, we allow s to vary independently of ε.

We separate different detachment processes by $\mathbf{B}$ and $\mathbf{C}$ because $\mathbf{A}+\varepsilon\mathbf{B}$ is the transition matrix of a reversible Markov process, while the $s\mathbf{C}$ process describes full detachment into an absorbing state, disrupts reversibility. $\mathbf{A}$ represents the binding reactions and is upper triangular with eigenvalues $\{0, -1, \cdots, -1, -2, \cdots, -2\}$; hence, the dimensionless eigenvalues of $\mathbf{W}(0) \equiv \mathbf{A}+\varepsilon\mathbf{B}$ fall into three groups:

- $\{\lambda : \lambda \sim O(\varepsilon) \lesssim 0\}$, unique;

- $\{\lambda : \lambda \sim -1 + O(\varepsilon)\}$, degeneracy $2(N-1)$;

- $\{\lambda : \lambda \sim -2 + O(\varepsilon)\}$, degeneracy $\frac{(N-2)(N-1)}{2}$.

These groups of values are mainly controlled by the "on-rate" transition matrix $\mathbf{A}$ and control the pattern of the eigenvalues of the full matrix $\mathbf{W}(s) = \mathbf{A} + \varepsilon\mathbf{B} + s\mathbf{C}$. Fig. 3 shows numerically computed eigenvalues of $\mathbf{W}$ for different values of $s = \varepsilon$. For sufficiently small ε, they fall into the three clusters governed by $\mathbf{A}$.
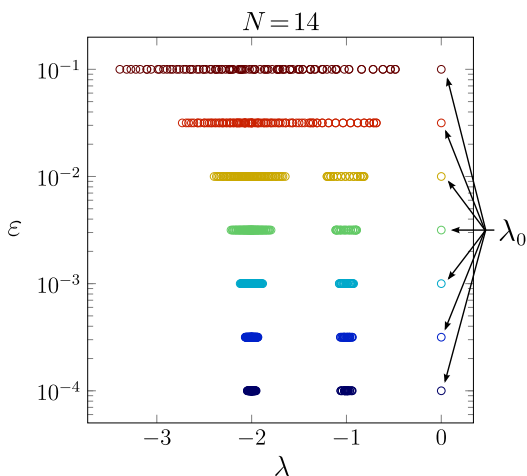
FIG. 3. Eigenvalues λ of the dimensionless transition matrix $\mathbf{W} = \tilde{\mathbf{W}}/k_{\mathrm{on}}$ associated with Ω for $N = 14$ and $\varepsilon = s = 0.1, 0.03, 0.01, 0.003, 0.001, 0.0003,$ and 0.0001. The principal dimensionless eigenvalues are $\lambda_0 \lesssim 0$, while two other groups cluster near -1 and -2 as $\varepsilon \to 0$.

The principal eigenvalue of $\mathbf{W}$, λ_0, can be computed using a two-step perturbation analysis. Adding $\varepsilon\mathbf{B}$ to $\mathbf{A}$ yields the matrix $\mathbf{W}(0) \equiv \mathbf{A} + \varepsilon\mathbf{B}$, which represents the internal transitions of the bound states Ω, and as such, has a unique eigenvalue 0 and an associated equilibrium distribution $\mathbf{v}_0$ as its eigenvector. Such internal transitions make the system an irreducible and reversible Markov process. Therefore, the equilibrium distribution $\mathbf{v}_0$ can be found as $v_0(n_1, n_2) \propto \varepsilon^{n_1+n_2}$, with $v_0(n_1, n_2)$ indicating the component of $\mathbf{v}_0$ on the element $(n_1, n_2) \in \Omega$. This scaling relation indicates that for small ε, the most probable states are those with small $n_1 + n_2$ (fully wrapped histones).

Applying perturbation theory to calculate the principal eigenvector $\mathbf{v}_0$ as a function of s, $\mathbf{v}_0(s)$, under the small change $\mathbf{W}(0) \to \mathbf{W}(0) + s\mathbf{C}$, one can see that each component of $\mathbf{v}_0(s)$ is approximately $v_0(n_1, n_2; s) = (1 + O(s))v_0(n_1, n_2; 0)$, as shown by Eq. (A20) in Appendix A 2. Consequently, the eigenvalue structure of the perturbed matrix $\mathbf{W}(0)+s\mathbf{C}$ is preserved not only for $s \ll \varepsilon$, but also for $s \sim \varepsilon$. Hence, we can use the principal eigenvector $\mathbf{v}_0(0)$ at equilibrium to approximate the principal eigenvector under the perturbation $s\mathbf{C}$. This procedure of switching on an absorbing boundary on an otherwise equilibrium system is commonly used to evaluate FPTs of rare events, usually known as the *absorbing boundary method* or generalized Fermi's Golden rule[29]. In the $\varepsilon, s \to 0^+$ limit, we find (see Eq. (A18) in Appendix A 2) the dimensionless principal (largest) eigenvalue of the perturbed matrix $\mathbf{W}(s) = \mathbf{W}(0) + s\mathbf{C}$ to be approximately

$$\lambda_0(s) = -Ns\varepsilon^{N-1}\big[1 + O(s)\big]. \qquad (2)$$

After reintroducing the physical rate k_{on}, the eigenvalue $\tilde{\lambda}_0 = k_{\mathrm{on}}\lambda_0$ associated with $\tilde{\mathbf{W}}$ sets the slowest physical timescale representing the effective rate of detachment from an equilibrium state. Eq. (2) can be motivated by considering the barrier-crossing rate or probability flux , i.e. the transition rate multiplied by corresponding equilibrium probability, from an equilibrium state to the detached state Ω^*. The energy barrier confining the equilibrium state is $(N-1)E_{\mathrm{c}}$ while there are N transition states. Therefore, the probability flux of disassembly is $\sim Nk_{\mathrm{d}}e^{(N-1)E_{\mathrm{c}}}$, which corresponds to a dimensionless principal eigenvalue of $Ns\varepsilon^{N-1}$.

The other eigenvalues $\lambda_{i>0}$ are ordered as $\lambda_0 \gg \lambda_1 \geq \cdots \geq \lambda_{\|\Omega\|}$. These other eigenvalues reflect the faster timescales associated with other states (eigenvectors). The difference between the principal eigenvalue and other eigenvalues, the *spectral gap*, is an important indicator of the dynamics of the system. If the system starts in any initial configuration in Ω, and the spectral gap is very large, it will quickly (with rate $\sim |\lambda_{i>0}|$) reach the near-equilibrium state $\mathbf{v}_0$ before ultimately dissociating with rate $|\lambda_0|$. As a result, the mean first passage time (MFPT) from any initial bound state $\mathbf{x}$ (such as $\mathbf{v}_0$) to the fully detached state Ω^* can be approximated by finding the MFPT that is dominated by the time from $\mathbf{v}_0$ to Ω^*. We find *the mean dimensionless nucleosome disassembly time* (the MFPT)

$$\mathbb{E}\big[T(\mathbf{x})\big] \approx \frac{1}{|\lambda_0|} \simeq \frac{1}{Nse^{(N-1)E_c}} \approx \frac{1}{Ne^{NE_c}}, \qquad (3)$$

where the last approximation assumes $s \approx \varepsilon$. Theoretical justification and further discussion of this approximation are provided in Appendix A 3, where Eq. (3) is proved as Eq. (A26).

In the context of the histone problem, according to Li *et al.*[8], single histone-DNA binding sites are highly dynamic, with an opening rate $k_{\mathrm{off}} \sim 4s^{-1}$ and a closing rate $k_{\mathrm{on}} \sim 20 - 90s^{-1}$. According to Eq. (2), this leads to an effective mean overall disassembly rate of $|\tilde{\lambda}_0| \approx$

$k_{on}|\lambda_0| \simeq N k_{on} e^{-NE_c} \approx 4.6 \times 10^{-8} \text{s}^{-1}$, corresponding to a mean nucleosome disassembly time $\mathbb{E}[T(\mathbf{x})]/k_{on} \sim 15$ years. Typically, the disassembly rate is defined by the inverse of the MFPT from the bound state to the detached state. In the case of multiple bound states, it is not easy to define a simple measure of disassembly rate given the complexity of the dynamics. A reasonable choice is to consider the weighted average of MFPTs from all bound states, with weights given by the (quasi-)equilibrium distribution of the bound states, which leads to the strict identity between the disassembly rate and $1/|\lambda_0|$. For a proof of this identity, see Eq. (A21). Fortunately, in the histone disassembly model, as we have argued above, the MFPT from all bound states to the detached state are similar and thus $1/|\lambda_0|$ is a reasonable measure of the overall disassembly rate.

In light of the above estimate for $\mathbb{E}[T(\mathbf{x})]/k_{on}$, cells need to dynamically remodel their histone binding patterns during DNA replication and changes in gene expression, processes that occur on a much shorter timescale. Fortunately, a variety of intracellular remodeling factors, such as SWI/SNF-type ATPases[26,30–32], can catalyze this remodeling process. Next, we will extend our model to incorporate mechanisms of remodeling cofactors that can compete for DNA or histone contacts.

2. Remodeler-facilitated linear detachment

Regulation of histone-DNA binding and acceleration of disassembly by other proteins/cofactors can be achieved in two ways: (i) competitive binding of proteins may block reattachment of histone contact sites to DNA and (ii) cofactors may allosterically inhibit histone-DNA binding. Recent studies suggest that a number of DNA-binding proteins interact with the histone-DNA complex by competing for open contact sites[10,33–35]. Here, we model such a mechanism via ratcheted blocking mechanism whereby nucleosome remodeler proteins block rebinding of DNA, thereby facilitating disassembly. The second, allosteric mechanism can be modeled directly by modification of site binding and unbinding rates k_{on} and k_{off}. Therefore, allostery can be subsumed under the spontaneous disassembly model. In the following discussion, we will focus on the blocking mechanism and refer to the intervening cofactor as a nucleosome remodeler. We develop a model that can be applied both to proteins that slide along DNA and to those that directly bind and occlude DNA-histone contact sites. While most known nucleosome remodelers are ATPases that slide along DNA[30–32], our model is also intended to describe the general interaction between DNA-binding proteins and the nucleosome and to better understand why other proteins cannot effectively evict histones from DNA.

Assume nucleosome remodeler proteins compete with histones on the same DNA binding sites and have binding rates p_a and dissociation rates p_d, as illustrated in Fig. 1. Bound contact sites must detach before cofactors such as remodeling protein can bind. However, if a remodeler first binds to and occludes a DNA or histone contact site, this site is unavailable for histone reattachment or binding, promoting histone detachment. We describe the state of DNA-histone-remodelers by a four-integer tuple (m_1, m_2, n_1, n_2). In this enumeration, m_1 and m_2 are the rightmost and leftmost contact sites occluded by a remodeler protein measured from the left and right ends of the contact footprint. These remodelers can bind to either the histone or the DNA substrate as shown in Fig. 1. In the presence of bound remodeler proteins ($m_1 > 0$ and/or $m_2 > 0$), the remaining available sites for direct DNA-histone interactions will be reduced to $N - m_1 - m_2$. The associated state space of (n_1, n_2) is then reduced correspondingly. In the presence of bound remodelers, n_1 and n_2 now measure the unbinding progress of the histone octamer and represent the additional numbers of opened binding sites inward from the rightmost and leftmost remodeler binding site. In this notation, the fully detached state is visited only when $m_1 + n_1 + m_2 + n_2 = N$.

Since (m_1, m_2) accounts only for the most inwardly occluded contact sites, the information about remaining remodelers is not delineated in this state space $\Omega_p := \{(m_1, m_2, n_1, n_2) \in \mathbb{N}^4 : m_1 + m_2 + n_1 + n_2 < N\} \cup \Omega_p^* := \{(m_1, m_2, n_1, n_2) \in \mathbb{N}^4 : m_1 + m_2 + n_1 + n_2 = N\}$. In the following, we will use the subscript "p" to indicate quantities associated with the remodeler-facilitated disassembly model. Consequently, the full remodeler adsorption pattern is not fully captured by m_1 and m_2. Multiple cofactors could cooperatively bind (where a DNA-bound cofactor accelerates binding of another cofactor near it) and compete for open sites amongst themselves, leading to complex dynamics of assisted histone displacement. We can simplify the model by considering, e.g., stepwise increases of (m_1, m_2), in which case m_1, m_2 can only change by 1 at a time. This restriction is appropriate for remodelers that are motor proteins processing along DNA[24] and yields an overall upper bound to remodeler-facilitated disassembly rates. Since molecular motors such as SWI/SNF complexes typically attack nucleosomes from one side, we explicitly modify our formulae in Appendix B to account for one-sided peeling.

Within the undissociated state space Ω_p, the transition matrix $\mathbf{H}$ can be constructed from matrices defined in the previous section. Because of occlusion by remodelers, histone detachment can now occur after spontaneous separation of $n \leq N$ binding sites. We denote the spontaneous transition matrix with n binding sites as $\mathbf{W}_n$ and define $\mathbf{W}_{n:m}$ to be block diagonal with m $\mathbf{W}_n$s on the diagonal. By arranging the states (m_1, m_2, n_1, n_2) as described in Appendix C, the transition matrix $\mathbf{W}_p = \mathbf{W}_{N,p}$ can be written as

$$\mathbf{W}_{N,\mathrm{p}} = \begin{bmatrix} \mathbf{W}_N & \mathbf{0} & \cdots & \mathbf{0} \\ \mathbf{0} & \mathbf{W}_{N-1:2} & \ddots & \vdots \\ \vdots & \ddots & \ddots & \mathbf{0} \\ \mathbf{0} & \cdots & \mathbf{0} & \mathbf{W}_{1:N} \end{bmatrix} + \frac{p_\mathrm{a}}{k_\mathrm{on}} \begin{bmatrix} \mathbf{M}_N & \mathbf{0} & \cdots & \mathbf{0} \\ \mathbf{M}_{N-1,N} & \mathbf{M}_{N-1} & \ddots & \vdots \\ \vdots & \ddots & \ddots & \mathbf{0} \\ \mathbf{M}_{1,N} & \cdots & \mathbf{M}_{1,2} & \mathbf{0} \end{bmatrix} + \frac{p_\mathrm{d}}{k_\mathrm{on}} \begin{bmatrix} \mathbf{0} & \mathbf{G}_{N,N-1} & \cdots & \mathbf{G}_{N,1} \\ \mathbf{0} & \mathbf{G}_{N-1} & \ddots & \vdots \\ \vdots & \ddots & \ddots & \mathbf{G}_{2,1} \\ \mathbf{0} & \cdots & \mathbf{0} & \mathbf{G}_1 \end{bmatrix}. \quad (4)$$

In Eq. (4), the states are grouped by the sum of $m_1 + m_2$ in ascending order. The first block entry represents the states with no remodeler bound, the second block entry represents the states with one remodeler bound, and so on. The transition matrices $\mathbf{M}_{m,n}$ and $\mathbf{G}_{m,n}$ describe changes in state associated with remodeler binding and unbinding, respectively, and the explicit construction rules of $\mathbf{W}_{N,\mathrm{p}}$ are given by Eqs. (C2-C4) in Appendix C. Specifically, column sums of $\mathbf{M}_{m,n}$ and $\mathbf{G}_{m,n}$ are zero, reflecting conservation of probability. We will again employ perturbation theory to find approximations for the principal eigenvalue. The unperturbed process corresponds to $p_\mathrm{a} = p_\mathrm{d} = 0$. Even though there are multiple eigenvectors associated with the eigenvalue 0 of the matrix $\mathbf{W}_{N,\mathrm{p}}$ with $p_\mathrm{a} = p_\mathrm{d} = 0$, we are interested only in the eigenvector that embeds the previous eigenvector $\mathbf{v}_0$ of $\mathbf{W}_N$. The embedding is implemented by appending zeros to the end of the original $\mathbf{v}_0$. This new $\mathbf{v}_0$ serves as the starting point of our subsequent perturbation analysis.

We will classify scenarios based on the ability of remodelers to occlude a binding site, defined by the remodeler-DNA binding energy $E_\mathrm{p} = \log(p_\mathrm{d}/p_\mathrm{a})$. An $E_\mathrm{p} > 0$ indicates $p_\mathrm{d} > p_\mathrm{a}$ and a weakly binding remodeler; negative $E_\mathrm{p} < 0$ means an attractive remodeler-DNA interaction and strong remodeler binding. Remodeler proteins compete directly with histones for DNA contact sites; this competition is quantified by comparing E_p to E_c. If $E_\mathrm{p} > E_\mathrm{c}$, histone-DNA binding is *stronger* than remodeler binding; if $E_\mathrm{p} < E_\mathrm{c}$, histone-DNA binding is weaker than remodeler binding. The complex state space and parameters of this problem, however, do not allow for simple analytical solutions.

Weak remodelers - In the the weak remodeler binding limit ($E_\mathrm{p} > E_\mathrm{c}$), the eigenvector corresponding to the largest eigenvalue is only weakly perturbed by the presence of remodelers but we can still use the total binding energy $E(m_1, m_2, n_1, n_2) = [(m_1 + m_2)(E_\mathrm{p} - E_\mathrm{c}) - (n_1 + n_2)E_\mathrm{c}]$ associated with each state (m_1, m_2, n_1, n_2) to approximate the steady state distribution $\mathbf{v}_0$ via the Boltzmann relation $v_0(m_1, m_2, n_1, n_2) \propto e^{-E(m_1, m_2, n_1, n_2)}$[36]. The principal eigenvalue can be found by via relation

$$\begin{aligned} \lambda_0 &= \frac{\mathbf{1}^\intercal \mathbf{W}_{N,\mathrm{p}} \mathbf{v}_0}{\mathbf{1}^\intercal \mathbf{v}_0}, \\ &\approx \frac{\sum_{(\mathbf{m},\mathbf{n})} \sum_{(\mathbf{m}',\mathbf{n}')} W_{N,\mathrm{p}}(\mathbf{m}',\mathbf{n}',\mathbf{m},\mathbf{n}) e^{-E(\mathbf{m},\mathbf{n})}}{\sum_{(\mathbf{m},\mathbf{n})} e^{-E(\mathbf{m},\mathbf{n})}}, \end{aligned} \quad (5)$$

where $(\mathbf{m}, \mathbf{n})$ represents the tuple (m_1, m_2, n_1, n_2) and $(\mathbf{m}', \mathbf{n}')$ represents the tuple (m_1', m_2', n_1', n_2').

$W(\mathbf{m}', \mathbf{n}', \mathbf{m}, \mathbf{n})$ represents the transition rate from state $(\mathbf{m}, \mathbf{n})$ to state $(\mathbf{m}', \mathbf{n}')$.

We proceed to simplify the expression in Eq. (5). At steady state, the most probable configuration is fully bound: $(m_1, m_2, n_1, n_2) = (0, 0, 0, 0)$, and other states are much less likely. The boundary states with positive transition rate to full disassembly are characterized by the condition $m_1 + m_2 + n_1 + n_2 = N - 1$. States $(\mathbf{m}, \mathbf{n})$ away from the boundary satisfies $\sum_{(\mathbf{m}',\mathbf{n}')} W(\mathbf{m}', \mathbf{n}', \mathbf{m}, \mathbf{n}) = 0$ because of conservation of probability. States $(\mathbf{m}, \mathbf{n})$ on the boundary satisfies $\sum_{(\mathbf{m}',\mathbf{n}')} W(\mathbf{m}', \mathbf{n}', \mathbf{m}, \mathbf{n}) = -s$. When $E_\mathrm{p} > 0$, the most probable boundary states are still those with $m_1 = m_2 = 0$ and $n_1 + n_2 = N - 1$, whose probability is proportional to $e^{(N-1)E_\mathrm{c}}$. When $E_\mathrm{p} < 0$, the most probable boundary states become those with $m_1 + m_2 = N - 1$ and $n_1 = n_2 = 0$, whose probability is proportional to $e^{(N-1)(E_\mathrm{c} - E_\mathrm{p})}$. In both cases, there are N identical most-probable boundary states because the attack comes from both ends, forming a triangular state space. Instead of investigating every state $(\mathbf{m}, \mathbf{n})$, we simplify the expression in Eq. (5) by considering only the state $(0, 0, 0, 0)$ with energy 0 and relative weight 1, and N boundary states with energy $(N-1)(E_\mathrm{p}^- - E_\mathrm{c})$ and weight $e^{(N-1)(E_\mathrm{p}^- - E_\mathrm{c})}$. Here, $E_\mathrm{p}^- := \min\{E_\mathrm{p}, 0\}$ to account for different most-probable boundary states under different conditions. With this approximation, we derive a physical estimate of the principal eigenvalue by summing Eq. (5) over the $N + 1$ most probable states in the interior and on the boundary

$$\lambda_0 \approx \hat{\lambda}_0(E_\mathrm{p} > E_\mathrm{c}) := -\frac{sN e^{(N-1)(E_\mathrm{c} - E_\mathrm{p}^-)}}{1 + N e^{(N-1)(E_\mathrm{c} - E_\mathrm{p}^-)}}. \quad (6)$$

If $E_\mathrm{p} > 0$, Eq. (6) reduces to the spontaneous disassembly rate given in Eq. (2) (since $E_\mathrm{c} \ll -1$). A more refined approximation of Eq. (5) that sums over more states is provided in Eq. (C12).

Strong facilitation limit – In the $E_\mathrm{p} \to -\infty$ limit, corresponding to irreversible remodeler binding ($p_\mathrm{d} \to 0$), the structure of the principal eigenvector $\mathbf{v}_0$ embedded in Ω_p is preserved under small a perturbation ($p_\mathrm{a} \ll k_\mathrm{on}$) as shown in Eq. (C8),

$$\mathbf{v}_0(p_\mathrm{a}) = \left[1 + O(\varepsilon) + O\left(\frac{p_\mathrm{a}}{k_\mathrm{on}}\right)\right] \mathbf{v}_0(0). \quad (7)$$

We can then use $\mathbf{v}_0(p_\mathrm{a})$ in the relation $\mathbf{v}_0^\intercal \mathbf{W}_{N,\mathrm{p}} \mathbf{v}_0 = \lambda_0 \|\mathbf{v}_0\|_2^2$ to extract an estimate of dimensionless principal

eigenvalue (see Eq.(C9))

$$\hat{\lambda}_0(E_{\mathrm{p}} \to -\infty, p_{\mathrm{a}} \ll k_{\mathrm{on}})$$

$$:= -\left[Nse^{(N-1)E_{\mathrm{c}}} + \frac{p_{\mathrm{a}}}{k_{\mathrm{on}}} \sum_{j=1}^{N-1} (j+1)e^{jE_{\mathrm{c}}} \right], \quad (8)$$

valid when $p_{\mathrm{a}} \ll k_{\mathrm{on}}$.

When $p_{\mathrm{a}} \sim k_{\mathrm{on}}$, the most probable state moves to the boundary since one may consider $p_{\mathrm{d}} = 0$ as a limit of $E_{\mathrm{p}} \to -\infty$, in which case the boundary states carry the lowest energy. Although the probability distribution is no longer proportional to e^{-E}, it provides intuition for the behavior of the system in this limit. The rate-limiting step is the one-step unbinding with rate k_{d}. Therefore, the perturbed principal eigenvalue $\lambda_0(p_{\mathrm{a}})$ is given by

$$\hat{\lambda}_0(E_{\mathrm{p}} \to -\infty) := \max\left\{ \hat{\lambda}_0(E_{\mathrm{p}} \to -\infty, p_{\mathrm{a}} \ll k_{\mathrm{on}}), -s \right\}. \quad (9)$$

Since the most probable state is shifted from those in the interior to those at the boundary, the principal eigenvalue approximates the inverse of the MFPT to Ω^* starting near the boundary. On the other hand, starting from the fully bound state, the system will first take an average time $(N-1)/k_{\mathrm{off}}$ to reach the boundary in the $p_{\mathrm{a}} \gg k_{\mathrm{on}}$ limit. Although MFPTs to the disassembled absorbing state differ for different initial configurations, for $E_{\mathrm{c}} \ll -1$ ($\varepsilon \ll 1$), they are all on the same order of magnitude determined by the unbinding rate k_{off} and k_{d}.

Effective facilitation – We have characterized the principal eigenvalue in the case of weak facilitation $E_{\mathrm{p}} > E_{\mathrm{c}}$ and strong facilitation limit $E_{\mathrm{p}} \to -\infty$. Of interest is the very typical intermediate case $E_{\mathrm{p}} < E_{\mathrm{c}}$ as it can effectively contribute to remodeling. However, in this limit, simple analytic approximations cannot be found, and we must compute the eigenvalues numerically. By using established numerical methods for evaluating the eigenvalues in `JuliaLang`[37], we find that the principal eigenvalue under intermediate $E_{\mathrm{p}} < E_{\mathrm{c}}$ is larger (smaller magnitude) than that of the strong facilitation limit $E_{\mathrm{p}} \to -\infty$ given by Eq. (9). The strong facilitation limit leads to shorter nucleosome disassembly times. Moreover, the right-hand side of Eq. (6) can be identified as approximately the probability flux intensity $j(\Omega_{\mathrm{p}}^* | \Omega_{\mathrm{p}}) := \sum_{\mathbf{x} \in \Omega_{\mathrm{p}}, \mathbf{y} \in \Omega_{\mathrm{p}}^*} W_{\mathbf{y},\mathbf{x}} v_0(\mathbf{x}) / \sum_{\mathbf{x} \in \Omega} v_0(\mathbf{x})$ into the detached state Ω_{p}^* from a quasiequilibrium configuration $\mathbf{v}_0$ in Ω_{p}. It is well-known that the principal eigenvalue is always dominated by the flux intensity[38]. Consequently, we can obtain an overall upper bound on the facilitation effect as the maximum of the two analytic approximations given by Eqs. (6) and (9):

$$\hat{\lambda}_{0,\mathrm{p}} := \max\left\{ \hat{\lambda}_0(E_{\mathrm{p}} > E_{\mathrm{c}}), \hat{\lambda}_0(E_{\mathrm{p}} \to -\infty) \right\}. \quad (10)$$

Further mechanistic insight can be gained via a coarse-grained model shown in Fig. 4, that ignores the fine structure of histone-DNA interaction by projecting the original undissociated state space $\Omega_{\mathrm{p}} = \{(m_1, m_2, n_1, n_2) :$

$m_1 + m_2 + n_1 + n_2 < N\}$ onto $\widetilde{\Omega}_{\mathrm{p}} := \{(m_1, m_2) : m_1 + m_2 < N\}$. Justification of this approximation is provided in Appendix A 3 while Appendix C 4 provides some physical intuition and discussion. Since we now track the transition of the states of only the nucleosome remodelers, the structure of this coarse-grained model resembles the original spontaneous linear detachment model, as shown in Fig. 4(a), where the effective rates p_{d} and $p_{\mathrm{a}}e^{E_{\mathrm{c}}}$ can be intuitively explained by considering the fine structure within a coarse-grained state shown in Fig. 4(b).
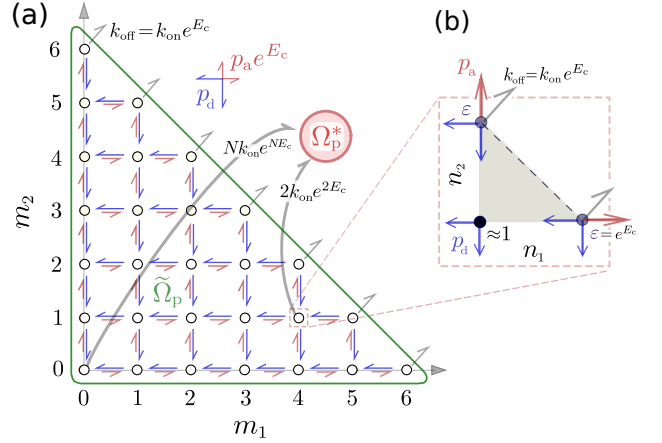
FIG. 4. A simple coarse-grained approximation of the *facilitated* intact-histone model. (a) The state space $\widetilde{\Omega}_{\mathrm{p}}$ and Ω_{p}^* for the coarse-grained model for the linear facilitated detachment. Each node represents the DNA occupancy (m_1, m_2) of remodeling factors. Red and blue arrows represent effective transitions corresponding to invading and retreating leading remodelers, respectively. The gray arrows (not all shown) represent the transition from the coarse-grained state (m_1, m_2) to the fully dissociated state Ω_{p}^* with rate $(N - m_1 - m_2)k_{\mathrm{on}}e^{(N-m_1-m_2)E_{\mathrm{c}}}$, where we have assumed $k_{\mathrm{d}} = k_{\mathrm{off}}$. (b) An illustration of the "internal structure" $\{(n_1, n_2) : n_1 + n_2 \leq 1\}$ within a coarse-grained state (m_1, m_2) in which $m_1 + m_2 = N - 2$. The internal dynamics are much faster than the transitions to external states indicated by different arrows in the schematic. The fast internal state is well characterized by a quasi-steady state distribution $v_0(n_1 = 0, n_2 = 0) \approx 1$, $v_0(1, 0) \sim v_0(0, 1) \approx \varepsilon = e^{E_{\mathrm{c}}}$, effectively lumping the state space shown in Fig. 2(b) into one with two binding sites. The ε-probability states are allowed to transit to Ω_{p}^* with rate k_{off}, and remodelers may bind to the exposed DNA with rate p_{a} in this case. If the internal states are in $(0, 0)$, the remodeler cannot bind to DNA and no direct transition to Ω_{p}^* is allowed. In all these states, the bound remodeler may detach with rate p_{d}. Multiplying the steady state probability of the internal structure and the corresponding transition rate yields the effective transition rates shown in (a). For example, binding of additional remodelers to DNA requires exposed DNA. Therefore, transition to higher (m_1, m_2) is not allowed when the internal state is $(0, 0)$. The probability of at least one site being exposed is $\sim e^{E_{\mathrm{c}}}$, resulting in an effective remodeler-DNA binding rate $p_{\mathrm{a}}e^{E_{\mathrm{c}}}$. For remodeler unbinding, there is no restriction on the internal state, and the effective unbinding rate is p_{d}.

Finally, to capture a crucial structural feature of histone-DNA interactions, we incorporate into the coarse-grained model an additional hopping rate from state (m_1, m_2) to the fully detached state $\Omega_{\rm p}^*$, given by $(N - m_1 - m_2)k_{\rm on}e^{(N-m_1-m_2)E_{\rm c}}$, assuming $k_{\rm d} = k_{\rm off}$. These hopping transitions to $\Omega_{\rm p}^*$ are inconvenient to visualize completely in Fig. 4(a), so we indicate only three effective transitions.

As shown in Fig. 5, we compare the numerical eigenvalues predicted by the coarse-grained model to those of the full model. The coarse-grained model approximates the original model well in all regimes of $E_{\rm p}$ provided $p_{\rm d} \ll k_{\rm on}$; however, analytic approximations to the principal eigenvalue are still inaccessible.
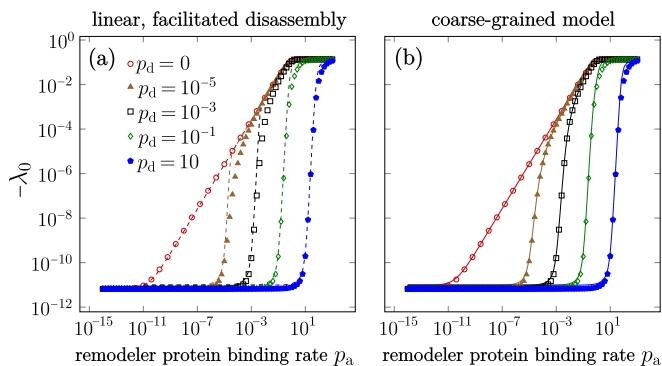
FIG. 5. Values of $-\lambda_0$ (principle eigenvalue of the transition matrix $\mathbf{H}_N$), a surrogate for the disassembly rate of nucleosome under remodeler facilitation, were numerically computed (symbols, both panels). (a) Numerically computed eigenvalues $-\lambda_0$ are compared to the approximation in Eq. (10) (dashed lines) using $E_{\rm c} = -2$. *Here, and in all subsequent plots, all rates are normalized with respect to $k_{\rm on}$.* (b) The same numerically computed values of $-\lambda_0$ are compared to the numerical predictions of the coarse-grained model (solid lines) indicating the accuracy of our coarse-graining.

Summarizing, our simplified model describing processive motors and nucleosome remodelers that bind strongly and cooperatively assumed stepwise transitions of (m_1, m_2). For remodelers that bind independently, the values of (m_1, m_2) can undergo longer-ranged jumps as multiple cofactors bind. Under quasi-steady state conditions, the probability of exposing Δm DNA-binding sites for remodeler binding is proportional to $e^{\Delta m E_{\rm c}}$; thus, the probability of increasing m_1 or m_2 by Δm due to remodeler binding is at most proportional to $e^{\Delta m E_{\rm c}}$. The probability of decreasing a certain number of sites depends on the position of the trailing remodelers and hence on the bulk remodeler concentration.

When remodeler binding is strong ($E_{\rm p}$ is very negative) or cooperative, m_1 and m_2 will seldom make large jumps so their dynamics can be treated as stepwise. On the other hand, when $p_{\rm a} \leq p_{\rm d}$, facilitation is minimal since the rate-limiting step is spontaneous peeling. Even for independent remodelers with weak binding energy, the

stepwise model predicts the numerically computed full-model disassembly rate reasonably well despite the possibility of large jumps to lower (m_1, m_2) states. Variances in our predictions under randomly distributed histone-DNA contact energies is considered in Appendix D. Remodelers that slide along DNA, such as DNA replication machinery, typically attack the nucleosome from outside the contact footprint.

B. Multimeric nucleosome disassembly model

In this section, we construct models of multistep disassembly nucleosomes composed of multicomponent histones. In solution, free histones exist in the form of $(H3\text{-}H4)_2$ tetramers and H2A-H2B dimers[39]. The tetramer is located at the center of the nucleosome and binds to around 60 base-pairs of nucleosomal DNA. Two identical H2A-H2B dimers align almost symmetrically at the two ends of the $(H3\text{-}H4)_2$ tetramer, each taking up around 30 base-pairs of nucleosomal DNA. The termini of H3 also attach to the DNA on both ends, further stabilizing the nucleosome complex[40].

Due to the multicomponent nature of the histone octamer, interesting questions arise as to whether: (i) octamer breakdown precedes histone-DNA detachment and (ii) whether the former process facilitates the latter. Studies have consistently shown that salt-induced disassembly of nucleosomes occurs stepwise, with H2A-H2B dimers disassembling first, followed by disruption of the $(H3\text{-}H4)_2$ tetramer as a whole[41–44]. However, nucleosome disassembly under physiological salt concentrations has yet to be observed due to the long timescales required.

Here, we propose a kinetic model that captures the multimeric feature of histone octamers and derive mean times of disassembly. We also consider the interaction between multimeric histone and nucleosome remodelers and show that by disrupting the interaction between $(H3\text{-}H4)_2$ and H2A-H2B, the detachment process can be significantly accelerated compared to the spontaneous, intact histone model. This observation is consistent with previous experimental results[45]. Interestingly, we also observe that the acceleration provided by octamer disassembly and nucleosome remodelers is sub-additive. By comparing the multimeric nucleosome disassembly model to the linear sequential disassembly model, we can predict disassembly pathways under various conditions. The multimeric is visualized in 6 and detailed below.

As discussed in the beginning of this subsection, we simplify the structure of the histone octamers as a concatenation of two (H2A-H2B) dimers on both ends of one $(H3\text{-}H4)_2$ tetramer in the center, as shown in Fig. 6(a). To enumerate the presence of the three different subunits and the links among them, we use the string $(\sigma_{\rm l}, \theta_{\rm l}, \sigma_{\rm m}, \theta_{\rm r}, \sigma_{\rm r}) \in \{0,1\}^5$ to represent the state of the histone complex. Here, $\sigma_j \in \{0,1\}$, $j \in \{\rm l, m, r\}$ represents whether the left, middle, or right part of the histone modules are present in the complex, while $\theta_i \in \{0,1\}$, $i \in$
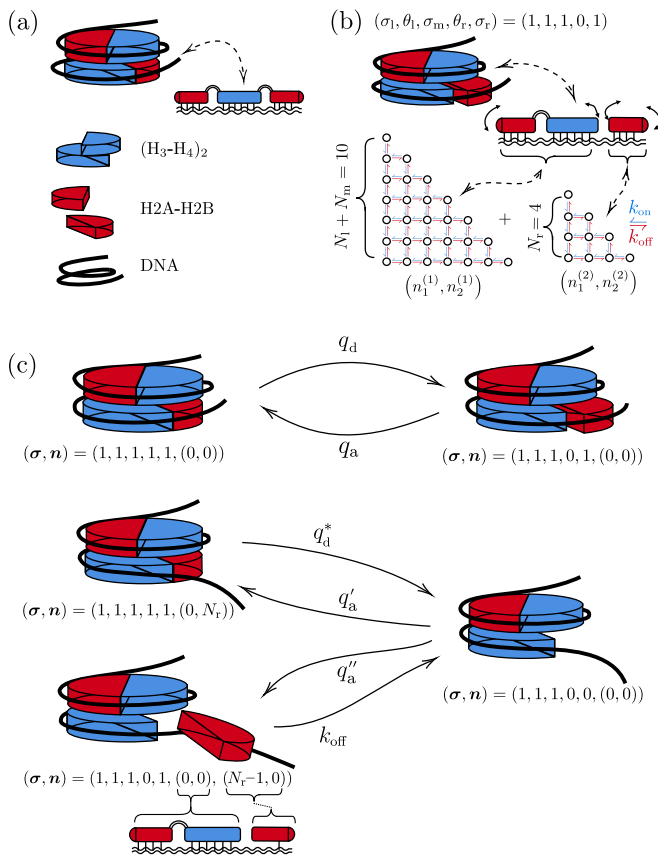
FIG. 6. Schematic of the multimeric nucleosome disassembly model. (a) A histone octamer is composed of one $(H3\text{-}H4)_2$ tetramer surrounded by two H2A-H2B dimers. The presence or absence of the three subunits is described by $(\sigma_l, \sigma_m, \sigma_r) \in \{0,1\}^3$, while links between them are described by $(\theta_l, \theta_r) \in \{0,1\}^2$. These are combined into the string $\boldsymbol{\sigma} = (\sigma_l, \theta_l, \sigma_m, \theta_r, \sigma_r) \in \{0,1\}^5$. Binding between the subunits and DNA is denoted by the vector $\mathbf{n}$ describing the peeling of contact footprints for each linked subunit cluster. (b) An example of the parameterization $(\boldsymbol{\sigma}, \mathbf{n})$ of state space. Here $\boldsymbol{\sigma} = (1,1,1,0,1)$ represents the macrostate where all subdomains of the histone bind to DNA but only one link exists among them. This leads to two independent linear detachment processes denoted by the microstate $\mathbf{n} = ((n_1^{(1)}, n_2^{(1)}), (n_1^{(2)}, n_2^{(2)}))$. In this particular case, breaking of the DNA-histone contacts can be initiated inside the total nucleosome footprint, at the interface between the right dimer and the tetramer, as indicated by the small solid-curve arrows. (c) Schematic representation of transitions associated with changes in θ_r, σ_r, and $\mathbf{n}$. For example, $(1,1,1,1,1,(0,0))$ represents the state where all subdomains are docked and fully bound to DNA and where the links between the tetramer and the dimers are intact.

$\{l, m\}$ indicates existence of links between the left and middle subunits and between the middle and right subunits, respectively. For any $\theta_i = 1$, both subunits that are linked together must be present.

Associated with each state of the histone $(\sigma_l, \theta_l, \sigma_m, \theta_r, \sigma_r)$ is a state space of "microstates"

that delineates the underlying states of DNA-histone bonds. The representation of microstates depends on the number $f = \sum_{i=l,m,r} \sigma_i - \sum_{j=l,r} \theta_j$ of independent histone modules (a single subunit or a bound cluster of subunits) that are *not* associated by a linkage. When the linkage is not present, unbinding of the DNA-histone contact sites can be initiated at the interface between a dimer and a tetramer. Each connected module then binds and unbinds independently in the same way as in the previous intact histone model, but with fewer contact sites on each module. Hence, each state is represented by a $2f$-tuple $(n_1^{(k)}, n_2^{(k)})_{k=1}^f$, where $n_1^{(k)}$ and $n_2^{(k)}$ are analogous to that defined in Fig. 2 and are the number of left- and right-detached contact sites of the kth histone module. For each k, $0 \leq n_1^{(k)} + n_2^{(k)} <$ number of DNA binding sites in the kth module. An example of macrostate $(\sigma_l, \theta_l, \sigma_m, \theta_r, \sigma_r) = (1,1,1,0,1)$ and associated microstates with $f = 2$ is shown in Fig. 6(b).

parameter/variable	symbol	value
left, middle, right subunit occupation	$\sigma_l, \sigma_m, \sigma_r$	$\{0,1\}$
no. of DNA-(H2A-H2B) binding sites	$N_l = N_r$	4
no. of DNA-$(H3\text{-}H4)_2$ binding sites	N_m	6
l-m and m-r subunit bonds	θ_l, θ_r	$\{0,1\}$
$(H3\text{-}H4)_2$-(H2A-H2B) association rate	q_a	-
$(H3\text{-}H4)_2$-(H2A-H2B) dissociation rate	q_d, q_d^*	$0.01 k_{on}$
$(H3\text{-}H4)_2$-(H2A-H2B) binding energy	$E_q = \log\left(\frac{q_d}{q_a}\right)$	-1
subunit chemical potential in solution	ΔE_s	2

TABLE II. Parameters and notation used the multimeric histone disassembly model. Three histone subunits can occupy the DNA substrate and are arranged as left (l), middle (m), and right (r). Their presence or absence is enumerated by $\sigma_l, \sigma_m, \sigma_r \in \{0,1\}$. The presence of the two possible subunit-subunit bonds are indicated by $\theta_l, \theta_r \in \{0,1\}$.

In the multimeric model, we assume that the bonds between H2A-H2B and $(H3\text{-}H4)_2$ can spontaneously break with rate q_d and rebind with rate q_a, provided at least one DNA-histone contacts is intact. However, once one of the domains loses all its bonds with DNA, the subunit is no longer held in place and its link with the neighboring histone domain may break at a somewhat different rate q_d^*. We also assume that each H2A-H2B carries $N_l = N_r = 4$ DNA binding sites and the central $(H3\text{-}H4)_2$ tetramer carries the remaining $N_m = 6$ contact sites. We do not distinguish different DNA binding sites and let them all have the same k_{on} and k_{off} as in our toy linear delamination model. The DNA-histone contact energy E_c is defined by $E_c = \log(\frac{k_{off}}{k_{on}}) < 0$ as before. An example of the macrostate transitions is shown in Fig. 6(c). The notation and parameters used in the multimeric model is given in Table II.

While it may be reasonable to assume $q_d^* > q_d$ (faster subunit dissociation if a subunit makes no DNA contacts), for the sake of simplicity, we will assume $q_d^* = q_d$ in the following discussion. We will also define the subunit binding affinity $E_q = \log(q_d/q_a)$ conditioned on the

presence of at least one DNA-histone contact for each of the subunits. Similarly, we also let $k_{\mathrm{d}} = k_{\mathrm{off}}$ in our subsequent calculations.

As discussed in the previous section, the disassembly rate depends on the choice of the initial state. If the initial state is chosen to be the quasi-steady state $\mathbf{v}_0$, then the disassembly rate is given by the principal eigenvalue $-\lambda_0$ of the relevant transition matrix. To numerically compute $-\lambda_0$, we constructed a computational algorithm to enumerate all the possible states and the associated transition matrix of the multimeric histone disassembly process. The principal eigenvalue was computed using the Arnoldi method[46]. The program is written in JuliaLang[37] and is available through GitHub at github.com/hsianktin/histone. We will also numerically compute the mean first disassembly times $\mathbb{E}[T(\mathbf{1})]$ of the multimeric model starting from the fully bound state $\mathbf{1}$. For a stochastic transition matrix $\mathbf{W}$, the $\mathbf{T} \equiv \mathbb{E}[T(\mathbf{x})]$ for all states $\mathbf{x} \in \Omega$ is found from solving $\mathbf{W}_\Omega^\intercal \mathbf{T} = -(1,\dots,1)^\intercal$ and then selecting $\mathbb{E}[T(\mathbf{x} = \mathbf{1})]^{47}$. Our subsequent results show that values of $-\lambda_0$ and $1/\mathbb{E}[T(\mathbf{1})]$ are close to each other because the most probable state $\mathbf{v}_0$ in the quasi-steady state coincides with the fully bound state $\mathbf{1}$.

If the concentration of free $(\mathrm{H3\text{-}H4})_2$ and H2A-H2B subunits in solution is negligible, we can treat the detachment of each subunit as irreversible. If there are appreciable concentrations of histone dimers or tetramers in solution, their rebinding to a partially disassembled nucleosome must be considered. An additional parameter $\Delta E_{\mathrm{s}}^{(\mathrm{subunit})} \equiv \log\left(k_{\mathrm{on}}/q_{\mathrm{a}}''^{(\mathrm{subunit})}\right)$ describing the free energy (or chemical potential) difference between specific subunits in solution and within a nucleosome is thus required; due to entropy, the higher the histone concentration, the lower this difference. The irreversible detachment of subunit corresponds to the $\Delta E_{\mathrm{s}} = \infty$ limit. A detailed analysis of reversible multimeric disassembly is given in Appendix E where dimers and tetramers in solution may rebind to a partially disassembled nucleosome, but the fully detached state is still absorbing in the first passage time setting. We will use subscript "q" to denote quantities relevant to the multimeric model.

1. Spontaneous detachment

We first consider the unfacilitated disassembly of a multimeric nucleosome and anticipate that subunit-subunit binding and unbinding rates, q_{a} and q_{d}, are much faster than their unbinding from DNA, the rate of which can be estimated by considering the disassembly rate of a simple intact-histone peeling model (Eq. 2) but with N_{l} binding sites: $k_{\mathrm{on}} N_{\mathrm{l}} e^{N_{\mathrm{l}} E_{\mathrm{c}}}$. Additionally, we assume that a fully linked histone is sufficiently stable so that our initial condition is an intact octamer. This assumption implicitly requires $q_{\mathrm{a}} > q_{\mathrm{d}}$ for self consistency and allows us to simply track unbinding from both ends of the octamer while ignoring the unbinding from the middle. It

takes an average dimensionless time $\tau_{\mathrm{H2A\text{-}H2B}} \approx e^{-N_{\mathrm{l}} E_{\mathrm{c}}}$ for the H2A-H2B on the left to unbind from the DNA, whether or not it is attached to the tetramer. This estimate is derived in Appendix B and comes from Eq. (B1) for the one-sided spontaneous linear nucleosome disassembly model with N_{l} binding sites. As with the two-sided spontaneous detachment model in Fig. 3, there is a large spectral gap between the first and second eigenvalues of the transition matrix. Therefore, the expected unbinding time starting from any bound configuration is given by the inverse of the principal eigenvalue and similar to that of the two-sided model. See the Appendix A 3 for details.
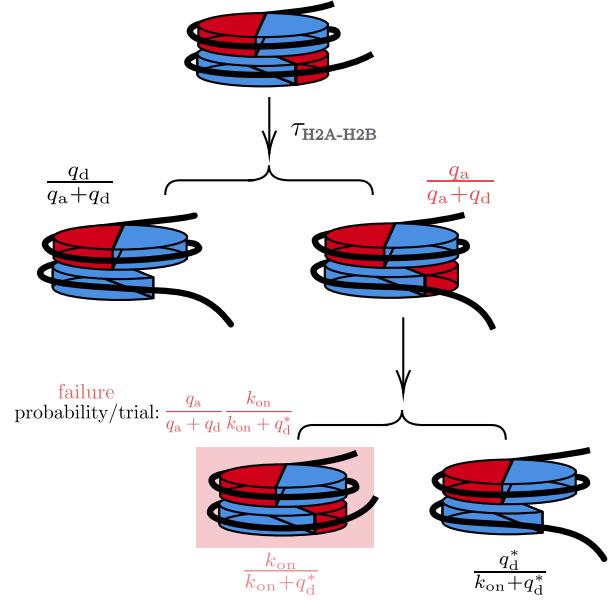
FIG. 7. Illustration of the geometric trial process. Dimer-DNA contacts break after about $\tau_{\mathrm{H2A\text{-}H2B}}$. When this happens the probability that the dimer-tetramer link is also broken is $q_{\mathrm{d}}/(q_{\mathrm{a}} + q_{\mathrm{d}})$. If this is realized, the dimer breaks free from the system. However, with probability $1 - q_{\mathrm{d}}/(q_{\mathrm{a}} + q_{\mathrm{d}}) = q_{\mathrm{a}}/(q_{\mathrm{a}} + q_{\mathrm{d}})$, the dimer-tetramer link is intact. From this configuration, there are two reactions competing with each other: the dimer rebinding to DNA with rate k_{on} and the dimer-tetramer link breaking with rate q_{d}^*, leading to the dimer breaking free from the system. Thus, the dimer rebinds to DNA with probability $k_{\mathrm{on}}/(k_{\mathrm{on}} + q_{\mathrm{d}}^*)$ (failing to disassociate) and breaks free with probability $q_{\mathrm{d}}^*/(k_{\mathrm{on}} + q_{\mathrm{d}}^*)$.

First, consider the expected time $\mathbb{E}[T]$ for the histone octamer to break down and its subunits to sequentially leave the system (the multimeric disassembly pathway) when rebinding does not occur (when the solution contains no free histone subunits and $\Delta E_{\mathrm{s}} = \infty$). Upon unbinding of H2A-H2B dimer from DNA, the chance that it is linked to the $(\mathrm{H3\text{-}H4})_2$ tetramer is $q_{\mathrm{a}}/(q_{\mathrm{a}} + q_{\mathrm{d}})$. If the H2A-H2B dimer is not bound to the tetramer $(\mathrm{H3\text{-}H4})_2$, it will immediately leave the system. Otherwise, there is a probability $k_{\mathrm{on}}/(k_{\mathrm{on}} + q_{\mathrm{d}}^*)$ that DNA and the dimer will rebind before the H2A-H2B dimer unlinks from $(\mathrm{H3\text{-}H4})_2$ and leaves the system. The expected time

for the H2A-H2B dimer to leave the system from a fully bound configuration $\mathbf{1} \equiv (1,1,1,1,1,(0,0))$ is thus given by

$$\mathbb{E}\big[T_{\text{H2A-H2B}}(\mathbf{1})\big] \approx \frac{e^{-N_l E_c}}{1 - \frac{q_a}{q_a+q_d}\frac{k_{on}}{k_{on}+q_d^*}}. \qquad (11)$$

Here, $1/\left(1 - \frac{q_a}{q_a+q_d}\frac{k_{on}}{k_{on}+q_d^*}\right)$ measures the expected number of trials until the H2A-H2B dimer leaves the system successfully, as illustrated in Fig. 7. When an attempt fails, the dimer-DNA contacts can quickly approach equilibrium because of the spectral gap for the simple peeling model. Thus, the next dimer removal trial occurs independently of the last one and the number of trials should follow a geometric distribution with the probability of failure given by $\frac{q_a}{q_a+q_d}\frac{k_{on}}{k_{on}+q_d^*}$. The expected time for both H2A-H2Bs to leave the system is on the same order of magnitude as the expected time for one H2A-H2B to leave the system.

After dissociation of the two equivalent dimers, the $(H3\text{-}H4)_2$ tetramer will unbind from the DNA at a rate of $k_{on} N_m e^{N_m E_c}$ according to Eq. (2) with N_m contact sites. We can then define the approximate expected time it takes for the entire nucleosome to detach through the multimeric breakdown pathway as

$$\mathbb{E}\widehat{[T(\mathbf{1})]} := \alpha \mathbb{E}\big[T_{\text{H2A-H2B}}(\mathbf{1})\big] + \frac{e^{-N_m E_c}}{N_m}, \qquad (12)$$

where $1 < \alpha < 2$ is an additional factor determining the expected MFPT for two independent dimers to detach. For independent, exponentially distributed waiting times, $\alpha = 3/2$. In our model, the dynamics of the dimers on opposite sides of the tetramer are independent, but their detachment times are modeled via a multistate geometric attempt processes, and are not exponentially distributed. Nonetheless, at this level of approximation $\alpha \sim 1$ suffices to to provide reasonable estimates.

The derivation of Eq. (12) implicitly assumes a sequential disassembly pathway where the H2A-H2B dimer disassemble first. Thus, Eq. (12) is valid only in the regime $q_a, q_d \gg k_{on} e^{N_l E_c}$.

Significant acceleration can be achieved if the links between the subunits are weak, thereby decreasing the $\mathbb{E}\big[T_{\text{H2A-H2B}}(\mathbf{1})\big]$ term in Eq. (12). When subunit links are weak ($E_q \ll -1 \Leftrightarrow q_d/(q_a+q_d) \not\sim 0$) and/or if unlinking is fast ($q_d^* \gg k_{on} \Leftrightarrow k_{on}/(k_{on}+q_d^*) \sim 0$), the factor $1/\left(1 - \frac{q_a}{q_a+q_d}\frac{k_{on}}{k_{on}+q_d^*}\right) \sim 1$ and thus $\mathbb{E}\widehat{[T(\mathbf{1})]} \approx e^{-N_m E_c}/N_m$.

Next, we relax the assumption that q_d and q_a are fast and introduce corrections to Eq. (12), obtaining a more general expression for the expected time for multimeric nucleosome dissociation. When the affinity between subunits is high ($E_q \ll -1$) and link breaking is slow ($q_d, q_d^* \ll k_{on}$), the mean nucleosome disassembly time of the system depends on the order of the term

$1/\left(1 - \frac{q_a}{q_a+q_d}\frac{k_{on}}{k_{on}+q_d^*}\right) e^{-N_l E_c}$. If $E_q \rightarrow -\infty$, to achieve mean nucleosome disassembly times comparable to the linear peeling model, we need $q_d^* < k_{on} e^{2N_l E_c}$, as shown by the purple symbols in Fig. 8(a). We assumed fast q_d^* in the derivation of Eq. (12). When q_d^* is not fast, the dissociation between histone subdomains can be a rate-limiting step in the multimeric pathway. In this case the total time required for the dimers to detach from the system is given by $\mathbb{E}[T_{\text{H2A-H2B}}] + k_{on}/q_d^*$. As indicated by the yellow and cyan symbols in Fig. 8(a), when $q_d^* < k_{on}/\mathbb{E}\widehat{[T(\mathbf{1})]}$, the rate of disassembly is proportional to q_d^*. When the dimer-tetramer unbinding rate further decreases to $q_d^* < k_{on} N e^{N E_c}$, the monomeric disassembly (simple histone peeling) is faster than multimeric breakdown and the dimensionless disassembly rate is $\approx N e^{N E_c}$ (for $k_d = k_{off}$).

Combining the above results, we obtain the following refined estimate for the dimensionless disassembly rate:

$$-\hat{\lambda}_{0,q}(\Delta E_s = \infty) := N e^{N E_c} + \frac{1}{\mathbb{E}\widehat{[T(\mathbf{1})]} + \frac{k_{on}}{q_d^*}} \qquad (13)$$

where $\mathbb{E}\widehat{[T(\mathbf{1})]}$ is the expected disassembly time in the $q_a, q_d \gg k_{on} e^{N_l E_c}$ limit given in Eq. (12). This formula provides a good qualitative description of both $1/\mathbb{E}[T(\mathbf{1})]$ and $-\lambda_0$ in the $\Delta E_s \rightarrow \infty$ limit (no subunit rebinding from bulk solution) as shown in Fig. 8(a). Additionally, we show close agreement between the numerically obtained principal eigenvalue λ_0 and the inverse of the mean dimensionless disassembly time starting from the fully bound state $\mathbf{1} = (\boldsymbol{\sigma} = (1,1,1,1,1), \mathbf{n} = (0,0))$.

When dimers and tetramers can rebind to a partially unwrapped nucleosome, with the fully detached state still absorbing in the first passage time problem, (finite histone subunit concentration in bulk, $\Delta E_s < \infty$), q_d^* still serves as a rate-limiting step for the multimeric breakdown pathway and the disassembly rate for small q_d^* can again be well approximated by the maximum of $N e^{N E_c}$ and q_d^*, as shown in Fig. 8(b). If q_d^* becomes moderately large, the problem can again be effectively be represented by an irreversible process that can be analyzed using the absorbing boundary method. Since the acceleration factor is approximately $e^{2(\Delta E_s + E_q)}$, disassembly is sped up only if $(\Delta E_s + E_q) \geq 0$. When $\Delta V/2 \equiv (\Delta E_s + E_q) + N_l E_c > 0$, the acceleration is limited by the rate of $(H3\text{-}H4)_2$ detachment, as shown in Fig. 8(c).

Appendix E 1 (Eq. (E9)) summarizes the above discussion and provides an estimate for the principal eigenvalue, and thus the mean disassembly time of the multimeric reversible ($\Delta E_s < \infty$) detachment model. Both multimeric and monomeric disassembly pathways are allowed in the full "multimeric" model, as illustrated in Fig. 9. The monomeric disassembly pathway usually occurs at a rate that is a lower bound to that of the multimeric disassembly pathway. Multimeric disassembly mediated by two dimer-tetramer links allows for stagewise
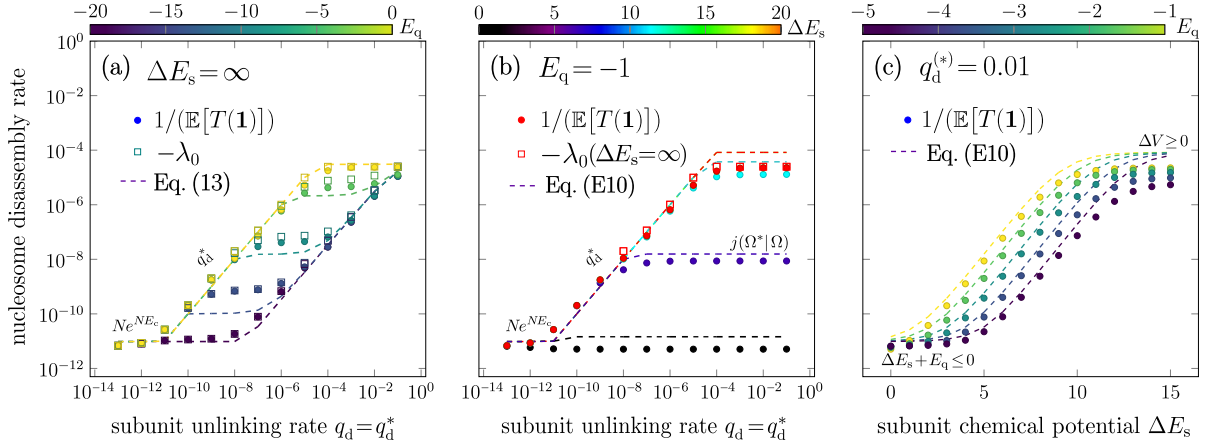
FIG. 8. Dimensionless rates of remodeler-free, multimeric nucleosome disassembly measured by the principal eigenvalue and the inverse of the dimensionless mean disassembly time $1/\mathbb{E}[T(\mathbf{1})]$. $-\lambda_0$ and $1/\mathbb{E}[T(\mathbf{1})]$ provide similar measures of the disassembly rate and agree well with each other as indicated in the plots. In all cases, we set $E_c = -2$, $k_d = k_{off}$, $q_d = q_d^*$, and all the rates are normalized by k_{on}. (a) Rates as a function of the dimensionless rate of subunit unlinking q_d^*/k_{on} in the zero bulk histone concentration ($\Delta E_s = \infty$) limit. Numerical results of the principle eigenvalue $-\lambda_0$ (open squares) closely match those of $1/\mathbb{E}[T(\mathbf{1})]$ (filled circles), indicating that starting from the fully DNA-bounded state or from the quasi-steady state yields similar mean dissociation times. All results are well approximated by the approximation $-\hat{\lambda}_{0,q}(\Delta E_s = \infty)$ for $-\lambda_0$ given in Eq. (13) (dashed curves). Other parameters are assigned typical values given in Tables I and II. (b) Comparison of $1/\mathbb{E}[T(\mathbf{1})]$ to the estimate $-\hat{\lambda}_{0,q}$ given in Eq. (E9). Here, we set $E_q = -1$, $\Delta E_s^{(H2A-H2B)} = \Delta E_s^{((H3-H4)_2)}$ and vary ΔE_s and $q_d = q_d^*$, which is the rate-limiting step as in (a). When $q_d < Ne^{NE_c}$, the disassembly rate is approximately Ne^{NE_c}. When $k_{on}Ne^{NE_c} < q_d < k_{on}j(\Omega^*|\Omega)$ (given by Eq. (E5)), the disassembly rate is controlled by q_d. When q_d/k_{on} is large, the dimensionless disassembly rate is approximated by $j(\Omega^*|\Omega)$. (c) Disassembly rates as a function of ΔE_s at different values of E_q for large (not rate-limiting) $q_d^*/k_{on} = 0.01$. Since $j(\Omega^*|\Omega) \sim N_m e^{NE_c+2(\Delta E_s+E_q)}$, larger $\Delta E_s + E_q$ leads to faster disassembly. The value of ΔE_s at which the disassembly rate saturates can be estimated by the root to $\Delta V \equiv 2(E_q + \Delta E_s + N_l E_c) = 0$. In this example, $N_l = 6, E_c = -2$, so when $E_q = -1$, the disassembly rate saturates at $\Delta E_s \approx 9$.
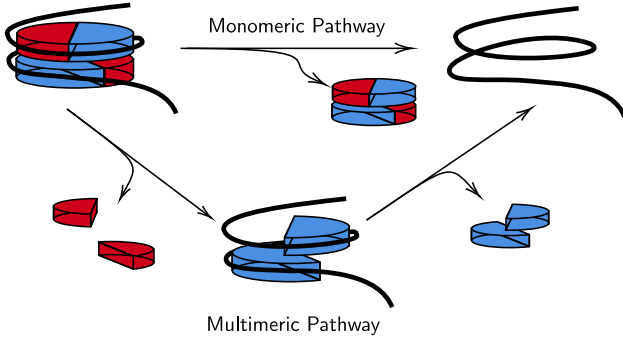
FIG. 9. Schematic of the two general pathways of nucleosome disassembly when the histone can break up into its subunits and detach separately.

dissociation of subunit-DNA contacts, accelerating the overall process compared to the intact histone disassembly model. Factors that limit the rate of multimeric pathways include the dissociation rate q_d^* and number of trials of dimer disassembly $1/\left(1 - \frac{q_a}{q_a+q_d}\frac{k_{on}}{k_{on}+q_d^*}\right)$ as described in Eq. (13). As detailed in Appendix F, the disassembly rate is approximated by a weighted sum of the rates associated with the monomeric and multimeric pathways, as depicted in Fig. 9. This means that disassembly in the

full multimeric model will always be faster than in simple intact-histone model in which only the monomeric pathway is present. By contrast, the multimeric disassembly pathway (conditioned on histone fragmentation) refers to the process where one histone module, dimer or tetramer, leaves the DNA before the whole histone complex dissociates from the DNA. This conditioned pathway can exhibit *slower* dissociation than that of the monomeric pathway, particularly when q_d^* is small.

2. Facilitated multimeric disassembly.

We now evaluate the interplay between remodelers and multimeric histones in the disassembly process. Even though interior octamer-DNA contacts can be transiently exposed for remodeler binding, for simplicity and tractability, we assume remodelers can only attack from the ends of the octamer-DNA contact footprint. This assumption changes the underlying geometry of the state space and is valid for describing the attack from motor proteins such as helicases and RNA polymerases. Since remodelers can attack only from the one exterior side of each H2A-H2B dimer, previous calculations of facilitated detachment in the linear peeling model can be readily adapted to the one-sided peeling model (see Appendix B). As in our analysis of the unfacilitated, irre-

versible multimeric model, the analysis in this section begins with the irreversible scenario ($\Delta E_s = \infty$). We first consider a dimer detaching from the system via a sequence of independent trials, each taking time $\tau_{\text{H2A-H2B}}$, followed by detachment of the remaining tetramer. Assuming the steady state approximation for each subdomain given by Eq. (B2) in Appendix B, we can estimate the dimensionless typical H2A-H2B dimer-DNA detachment time with possibility of tethering to the tetramer

$$\tau_{\text{H2A-H2B}} := \frac{1 + e^{(N_l - 1)(E_c - E_p^-)}}{\varepsilon e^{(N_l - 1)(E_c - E_p^-)}} \qquad (14)$$

in the weak remodeler regime. Here, Eq. (B2) is the one-sided version of Eq. (6) and its inverse results in the estimate for $\tau_{\text{H2A-H2B}}$ and illustrates how one can apply previous results from the simple, intact-histone peeling model to the peeling of each of the histone subunits by modifying the number of contact sites from N to N_l, N_r.

To obtain an estimate for both strong and weak remodeler regimes, we shall use the one-sided version of Eq. (10) by taking the maximum of Eq. (B2) and Eq. (B3). Following the arguments made for non-facilitated multimeric disassembly that led to Eq. 11, the probability $q_a/(q_a + q_d)$ that the dimer is still attached to the $(\text{H3-H4})_2$ tetramer after its DNA contacts are broken is now modified by the probability that contacts reform before dimer-tetramer bond breaking *in the presence of remodeler competition.* When there is a strong facilitation by remodelers, they will block DNA contact sites quickly after the histone dimer unbinds from these contact sites. Remodeler binding at rate p_a and dimer dissociation from the $(\text{H3-H4})_2$ tetramer occurring at rate q_d thus compete with H2A-H2B-DNA contact rebinding. Consequently, in the $q_a, q_d \gg k_{\text{on}} e^{N_l E_c}$ limit, the expected time for complete H2A-H2B dimer detachment from the nucleosome can be approximated by

$$\mathbb{E}\big[\widehat{T_{\text{H2A-H2B}}(\mathbf{1})}\big] := \frac{\tau_{\text{H2A-H2B}}}{\left(1 - \frac{q_a}{q_a + q_d} \frac{k_{\text{on}}}{k_{\text{on}} + p_a + q_d}\right)}. \qquad (15)$$

The expected dimensionless time for detachment of the remaining $(\text{H3-H4})_2$ tetramer is given by $\tau_{(\text{H3-H4})_2} \approx \big(1 + N_m e^{(N_m - 1)(E_c - E_p^-)}\big)/\big(\varepsilon N_m e^{(N_m - 1)(E_c - E_p^-)}\big)$, analogous to $\tau_{\text{H2A-H2B}}$ given in Eq. (14) and the inverse of $\hat{\lambda}_0(E_p > E_c)$ given in Eq. (6) for the weak facilitation limit, but with N_m tetramer-DNA contact sites. In analogy to the expected time for detachment of a multimeric nucleosome in the absence of remodelers (Eq. (12)), the expected dissociation time in the presence of remodelers can be estimated as the sum of the expected time for detachment of both H2A-H2B dimers and the $(\text{H3-H4})_2$ tetramer:

$$\mathbb{E}\big[\widehat{T(\mathbf{1})}\big] := \alpha \mathbb{E}\big[\widehat{T_{\text{H2A-H2B}}(\mathbf{1})}\big] + \tau_{(\text{H3-H4})_2}, \qquad (16)$$

valid in the $q_a, q_d \gg k_{\text{on}} e^{N_l E_c}$ limit.

In the strong facilitation limit, we simply replace the estimate of the DNA-detachment times $\tau_{\text{H2A-H2B}}$ and

$\tau_{(\text{H3-H4})_2}$ given in Eq. (16) by Eq. (B3) and Eq. (10), with N_l and N_m number of contact sites.
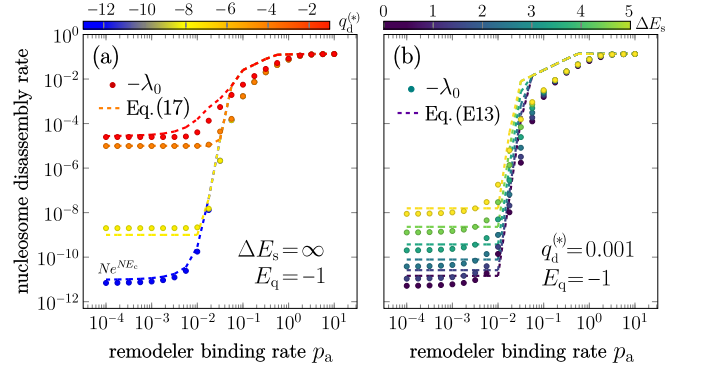
FIG. 10. Principal eigenvalues – an estimate of $1/\mathbb{E}[T(\mathbf{1})]$ – from the remodeler-facilitated disassembly model. (a) For the irreversible model (no subunits in solution), the dimensionless disassembly rate $-\lambda_0$ is plotted as a function of remodeler binding rate p_a, for fixed $E_c = -2$, $E_q = -1$, $p_d = 0.01$, with estimates given by Eq. (17) (b) The disassembly rate $-\lambda_0$ for different subunit chemical potential differences $\Delta E_s^{(\text{H2A-H2B})} = \Delta E_s^{(\text{H3-H4})_2} = \Delta E_s$. Estimates given in Eq. (E12) are plotted as the dashed curves which agree well with numerical results. In (a) and (b), $q_d = q_d^* \equiv q_d^{(*)}$ and all rates are normalized with respect to k_{on}.

Likewise, we can estimate the principal eigenvalue of the facilitated multimeric detachment process by considering the contributions from the monomeric, simple histone disassembly pathway and other rate-limiting steps:

$$-\hat{\lambda}_{0,\text{p,q}}(\Delta E_s = \infty) = -\hat{\lambda}_{0,\text{p}} + \frac{1}{\mathbb{E}\big[\widehat{T(\mathbf{1})}\big] + \frac{k_{\text{on}}}{q_d^*}}, \qquad (17)$$

where $\hat{\lambda}_{0,\text{p}}$ is given by Eq. (10) and provides an estimate of the rate of monomeric histone dissociation, while $\mathbb{E}\big[\widehat{T(\mathbf{1})}\big]$ is given by Eq. (16). Comparison between this estimate and numerical results are shown in Fig. 10(a). Note that the requirement $E_c - E_p^- > 0$ for effective facilitation remains the same as in the simple intact-histone model. When the remodelers bind weakly, histone fragmentation provides a strong facilitation to the detachment process. However, when remodelers bind strongly, histone fragmentation does not significantly accelerate disassembly.

The case of finite subunit concentrations in solution (finite ΔE_s) is discussed in more detail in Appendix E 2. An estimate of the disassembly rate is given in Eq. (E12). Analytic approximations and numerical results are compared in Fig. 10(b) and show qualitative agreement. Nucleosome remodelers facilitate the disassembly by reducing the energy barrier for each contact site. This facilitation acts somewhat independently from histone fragmentation so the threshold $E_p < E_c$ for effective facilitation is the same as that in the linearly peeling model, regardless of different values of ΔE_s and E_q.
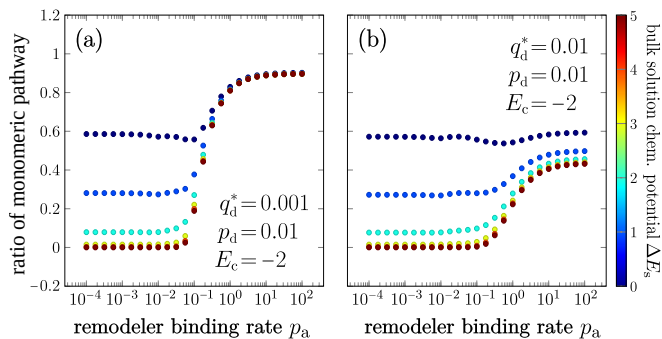
FIG. 11. The fraction of disassembly pathways that lead to dissociation of an intact histone octamer. This quantity is defined as the probability that the histone is an intact octamer at the moment of full nucleosome disassembly. (a) The probability of monomeric nucleosome disassembly is plotted as a function of remodeler binding p_a for different chemical potentials ΔE_s. Here a small subunit unbinding rate $q_d^* = 0.001$ and a large chemical potential (low subunit concentration in solution) allows for a sharp transition to a monomeric disassembly pathway as facilitation is increased through p_a. (b) The probability of monomeric disassembly plotted against p_a, but with $q_d^* = 0.01$. The larger unbinding rate increases the probability of a fragmented-histone disassembly. In (a) and (b) all rates are normalized by k_{on}.

As detailed in Appendix F, we also found that remodeler binding and histone subunit concentration in solution can conspire to bias the disassembly from a more fragmented dissociation pathway to one in which the histone complex dissociates intact. Fig. 11 shows the probability of the histone in an intact octamer state at the moment of full nucleosome disassembly. In the weak remodeler facilitation regime, low histone subunit concentration typically allows a faster multimeric disassembly pathway, while high histone subunit concentration makes the rates of monomeric and multimeric disassembly comparable. In the former case, the histone is more likely to dissociate after fragmentation. On the other hand, when the remodeler binding is strong, both pathways have similar rates. In this case, the probability of the histone dissociating as an intact octamer depends on the dimer-tetramer unbinding rate q_d^* and the dimensionless mean disassembly time under the multimeric fragmentation pathway $\widehat{\mathbb{E}[T(\mathbf{1})]}$. When $q_d^* < k_{on}/\widehat{\mathbb{E}[T(\mathbf{1})]}$ (but $q_a, q_d \gg k_{on}e^{N_1 E_c}$), the histone is more likely to dissociate as an intact octamer, as shown in Fig. 11(a). When $q_d^* \geq k_{on}/\widehat{\mathbb{E}[T(\mathbf{1})]}$ (and $q_a, q_d \gg k_{on}e^{N_1 E_c}$), it is more likely to fragment before complete dissociation, as shown in Fig. 11(b).

III. SUMMARY AND CONCLUSIONS

In this study, a suite of Markov chain models was developed to analyze nucleosome stability. We delineated a number of mechanisms that probably contribute to nucle-osome stability, including a model of multimeric histone disassembly.

Linear detachment model. Our first proposed mechanism maintains both high accessibility for few energy consuming proteins and low accessibility for generic DNA binding proteins. For the spontaneous detachment problem, the model can be described by a single parameter, the contact free energy E_c, which we assume $E_c \ll -1$ to reflect strong histone-DNA binding. The simple-histone linear peeling mechanism described by our first model applies not only to the histone detachment problem, but also to a family of nucleic acid-binding proteins that both protect the nucleic acid from attack and respond to regulation signals quickly. Examples include *E. coli* single-stranded DNA binding proteins (*E. coli* SSB) and replication protein A (RPA) that exists in eukaryotic cells.

In an extended model that incorporates remodeler-facilitated disassembly, we analyzed the enhancement of dissociation provided by processive motors moving along DNA, which also serves as a good estimate of facilitation by generic remodelers binding from solution. We introduced additional parameters that quantify the remodeler binding rate p_a and binding energy E_p. When the dissociation rate $p_d = p_a e^{E_p}$ is not too slow, a quasi-steady state approximation provides a tight upper bound on the effective unbinding rate, revealing a high degree of cooperativity and a gating mechanism sensitive to the energy cost of the processive motors or remodelers. Efficient acceleration is possible only if $E_c - E_p > 0$; this energy difference controls a "gate" that allows certain proteins like polymerases to access DNA while preventing generic DNA binding proteins from penetrating the nucleosome. This simple analysis helps resolve the paradox that histones must simultaneously bind tightly to DNA yet rapidly release DNA when accessibility is required, for example, during transcription or DNA replication. Our prediction is consistent with observations from previous single-molecule experiments and data-driven modeling that fast-diffusing remodelers in the absence of ATP consumption do not significantly affect the nucleosome disassembly rate[10].

Besides nucleosomes, are many other biologically important systems in which protein-DNA binding and unbinding arise[48]. Many have been studied in single-molecule experiments that interrogate the collective dynamics of proteins along a single DNA strand, where facilitated protein detachment was observed under increased protein concentration in solution[49,50]. Our simple-histone models may provide insight into developing models for these more general protein-DNA systems.

Multimeric detachment model. We also derived explicit formulae for mean first dissociation times of nucleosomes in which the histone is comprised of octamer subunits (two dimers and a tetramer). We first considered the irreversible histone detachment model in which once a histone subunit (dimer or tetramer) detaches from the nucleosome complex, it does not rebind. In a sponta-

neous, incremental detachment model, both the binding energy E_q between histone dimers and tetramers and their dissociation rates q_d are additional relevant parameters. The dimer-tetramer dissociation rate q_d can also depend on the state of the DNA-histone binding sites. We thus allow an additional parameter q_d^* to describe the unbinding rate when at least one of the histone modules is completely unbound from the DNA. Although binding affinities between histone subunits have not been experimentally characterized, we found that the detachment rate can be significantly upregulated by modulating the binding free energy E_q between the $(H3-H4)_2$ tetramer and the H2A-H2B dimers. This effect comports with the observation that mutations that reduce the binding affinity between different modules of histones lead to a much shorter disassembly time of around 20 minutes[45,51].

The case of reversible binding (exchange of subunits from bulk solution) is fully discussed in the Appendix, where we introduced additional parameters $\Delta E_s^{(subunit)}$ and q_a, q_a', q_a'' to describe the free energy difference between histone particles in solution and those bound to a nucleosome (not counting the associated subunit-DNA contacts) and rebinding rates. Kinetically, if a histone dimer fully detaches from DNA but is still linked to the DNA-bound tetramer, it is held close to the DNA, resulting in a locally high effective dimer concentration. Since dimers in solution are much more dilute, the binding rate should be much smaller than k_{on}. When free histones are present in the solution, the stability of the nucleosome can be modulated by the concentration of free histones. For example, a recent experiment reported that the free histone concentration is a key modulator of different responses of nucleosomes to the progression of replication fork[52]; our model can potentially be adapted to provide a mechanistic insight into this observation.

tachment model disassembles faster than the linear detachment model. However, strong nucleosome remodelers, high concentrations of free histones in solution, and strong binding between histone dimers and tetramers can render the multimeric disassembly pathway less likely.

All of our results are derived assuming uniform binding and unbinding rates between histone and DNA contacts, and are listed in Table III. Numerical tests of heterogeneous k_{off} performed in Appendix D suggest that disassembly of nucleosome that have *random* histone-DNA contact energy profiles (depending on DNA sequence) can be well characterized by the average binding energy. However, recent analysis suggest that these rates may exhibit cooperativity depending on the amount of unwrapped DNA[25]. Our model can be extended to capture such effects by allowing $k_{off}(n_1, n_2)$ to explicitly depend on the state of the system or by simply allowing k_{off} to be different constants for the H2A-H2B-DNA and $(H3-H4)_2$-DNA contacts.

Although our predictions focus on the mean time to disassembly of a single histone, higher moments or distributions of disassembly times can in principle be numerically extracted from our stochastic model. Our suite of models provide the building blocks for constructing higher-level models of rearrangement of interacting nucleosome assemblies[53–56] that occur during important cellular processes such as transcription and replication[57] and post-translational modification of histone binding energies[10,58].

AUTHOR DECLARATIONS

Conflict of Interest

The authors have no conflicts to disclose.

model	detachment method	$|\lambda_0|$
simple histone		
	spontaneous	Eq.(2)
	facilitated	Eq.(10)
	one-sided, spontaneous	Eq.(B1)
	one-sided, facilitated	Eq.(B4)
multimeric histone		
	irreversible spontaneous	Eq.(13)
	reversible spontaneous	Eq.(E9)
	irreversible facilitated	Eq.(17)
	reversible facilitated	Eq.(E10)

TABLE III. A summary of main analytical approximations developed in this paper.

Histones can disassemble from DNA either as a whole, or in a piecewise fashion. Our two classes of models represent two parallel pathways of nucleosome disassembly. The first pathway is defined by linear intact-histone detachment, while the second pathway reflects disassembly involving histone fragmentation. Preference of one pathway over the other depends on the subunit unlinking and remodeler binding rates. Typically, the multimeric de-

DATA AVAILABILITY

The data that support the findings of this study are available within the article.

object	symbol	examples
matrices and vectors	bold letters	$\mathbf{W}, \mathbf{P}(t), \mathbf{x}, \mathbf{n}...$
scalars, components of matrices and vectors	normal letters	$W_{ij}, P(n_1, n_2, t), x_i, n_1, n_2$
eigenvalues and eigenvectors sorted by real parts in descending order	$\lambda_i, \mathbf{v}_i$	$\lambda_0, \mathbf{v}_0, \lambda_1, \mathbf{v}_1, \cdots$
the state space for the undissociated histone	Ω	-
a state in the state space	$\mathbf{x}$	-
the state of the dissociated histone	Ω^*	-
vectors with all entries equal to a number	bold numbers	$\mathbf{1}, \mathbf{0}$
fully histone-DNA bound state with all contact sites closed	$\mathbf{1}$	$\mathbf{1}$
Euclidean inner product of two vectors	$\langle \cdot, \cdot \rangle$	$\langle \mathbf{x}, \mathbf{y} \rangle$
transpose of a vector or matrix	$.^\mathsf{T}$	$\mathbf{x}^\mathsf{T}, \mathbf{W}^\mathsf{T}$
dimensionless first passage time (FPT) starting from $x \in \Omega$ to detached state Ω^*	$T(\mathbf{x})$	$T(\mathbf{1})$
estimates for a quantity	hat over the symbol	$\hat{\lambda}_0, \widehat{\mathbb{E}[T(\mathbf{1})]}$
vectors with first row removed, or matrices with first row and column removed	$\bar{\cdot}$	$\bar{\mathbf{v}}, \overline{\mathbf{W}}$
quantities relevant to remodeler-facilitated models	subscript "p"	$\hat{\lambda}_{0,\mathrm{p}}, E_\mathrm{p}$
quantities relevant to multimeric histone models	subscript "q"	$E_\mathrm{q}, \hat{\lambda}_{0,\mathrm{q}}, \hat{\lambda}_{0,\mathrm{p},\mathrm{q}}$

TABLE IV. General nomenclature for mathematical symbols and objects.

Appendix A: Transition matrices, eigenvectors, and eigenvalues for the intact-histone, spontaneous detachment model

1. Transition matrix for the intact-histone, spontaneous detachment model

To simplify our mathematical analysis, we normalize all rates by k_on so that $k_\mathrm{off}/k_\mathrm{on} = \varepsilon, k_\mathrm{d}/k_\mathrm{on} = s$, and λ_i are dimensionless. It is straightforward to reconstruct physical rates and times by multiplying or dividing by k_on. We allow the total number of contact sites N to be a variable and relabel the transition matrix $\mathbf{W}$ as $\mathbf{W}_N \equiv \mathbf{A}_N + \varepsilon\mathbf{B}_N + s\mathbf{C}_N$, which can be generated recursively.

The exact form of transition matrix depends on how the different states (n_1, n_2) of Ω are enumerated. We choose to order states by first grouping ones with the same $n_1 + n_2$ together, then ordering the others by ascending order in $n_1 + n_2$. Finally, states in the same group are ordered in ascending n_1. For example, the first few states are $(0,0), (0,1), (1,0), (0,2), (1,1), \ldots$. This bookkeeping scheme allows us to construct the transition matrices via simple recursion. Setting $\mathbf{A}_1 = 0$, $\mathbf{A}_n$ is

$$
\mathbf{A}_n = \begin{bmatrix}
\mathbf{A}_1 & \mathbf{F}_1 & \mathbf{0} & \cdots & \cdots & \mathbf{0} \\
\mathbf{0} & \mathbf{D}_1 & \mathbf{F}_2 & \mathbf{0} & \cdots & \mathbf{0} \\
\mathbf{0} & \mathbf{0} & \mathbf{D}_2 & \mathbf{F}_3 & \ddots & \vdots \\
\mathbf{0} & \vdots & \ddots & \ddots & \ddots & \mathbf{0} \\
\mathbf{0} & \vdots & & \ddots & \ddots & \mathbf{F}_{n-1} \\
\mathbf{0} & \mathbf{0} & \cdots & \cdots & \mathbf{0} & \mathbf{D}_{n-1}
\end{bmatrix}, \qquad \text{(A1)}
$$

where $\mathbf{F}_k$ is a $k \times (k+1)$ matrix, with the two longest diagonals set to 1 (all other entries are zero), representing the closure of one open contact site. The matrix $\mathbf{D}_k = \mathrm{diag}\{-1, -2, -2..., -2, -1\}$ is a $(k+1) \times (k+1)$ diagonal matrix determined by setting the column sums of $\mathbf{A}_k$ to 0. By construction, $\mathbf{A}_N$ is a $\frac{N(N+1)}{2} \times \frac{N(N+1)}{2}$ upper triangular matrix with the diagonal entries $\{0, -1, \cdots, -1, -2, \cdots, -2\}$. Specifically, there is one diagonal entry with value 0, $2(N-1)$ diagonal entries with value -1, and the remaining $(N-1)(N-2)/2$ diagonal entries with value -2.

Elements in

$$
\mathbf{B}_n = \begin{bmatrix}
\mathbf{D}'_0 & \mathbf{0} & \mathbf{0} & \cdots & \cdots & \mathbf{0} \\
\mathbf{F}_1^\mathsf{T} & \mathbf{D}'_1 & \mathbf{0} & \cdots & \cdots & \mathbf{0} \\
\mathbf{0} & \mathbf{F}_2^\mathsf{T} & \mathbf{D}'_2 & \ddots & & \vdots \\
\mathbf{0} & \mathbf{0} & \ddots & \ddots & \ddots & \vdots \\
\mathbf{0} & \vdots & \ddots & \ddots & \mathbf{D}'_{n-2} & \mathbf{0} \\
\mathbf{0} & \mathbf{0} & \cdots & \mathbf{0} & \mathbf{F}_{n-1}^\mathsf{T} & \mathbf{0}
\end{bmatrix}. \qquad \text{(A2)}
$$

represent rates of transitions to higher $n_1 + n_2$. A simple way of defining $\mathbf{B}_n$ is to transpose $\mathbf{A}_n$ and change the diagonal terms so that each column adds up to 0 to conserve total probability. The reason why we can do this is that for every transition lowering $n_1 + n_2$, there is exactly one opposing transition raising $n_1 + n_2$. Since $\mathbf{W}_{ij}$ represents transition rate from state j to state i, we transpose the matrix to invert the direction of transition. In Eq. (A2), the matrix $\mathbf{F}_k^\mathsf{T}$ is the transpose of $\mathbf{F}_k$ and $\mathbf{D}'_k$ is a $(k+1) \times (k+1)$ diagonal matrix with all diagonal entries being -2. The last diagonal entry $\mathbf{0}$ is an $n \times n$ matrix with all entries being zero.

Finally, the matrix $\mathbf{C}_n$ represents the transitions leaving the state space into the absorbing states. For $n \in \mathbb{Z}_+$,

$$
\mathbf{C}_n = \begin{pmatrix} \mathbf{0} & \mathbf{0} \\ \mathbf{0} & -\mathbf{I}_n \end{pmatrix}, \qquad \text{(A3)}
$$

where $\mathbf{C}_n$ is an $\frac{n(n+1)}{2} \times \frac{n(n+1)}{2}$ matrix and $\mathbf{I}_n$ is the identity matrix in $\mathbb{R}^{n \times n}$.

To be concrete, the matrices $\mathbf{A}_3$, $\mathbf{B}_3$ and $\mathbf{C}_3$ are explicitly

$$\mathbf{A}_3 = \begin{pmatrix} 0 & 1 & 1 & 0 & 0 & 0 \\ 0 & -1 & 0 & 1 & 1 & 0 \\ 0 & 0 & -1 & 0 & 1 & 1 \\ 0 & 0 & 0 & -1 & 0 & 0 \\ 0 & 0 & 0 & 0 & -2 & 0 \\ 0 & 0 & 0 & 0 & 0 & -1 \end{pmatrix}, \quad \mathbf{B}_3 = \begin{pmatrix} -2 & 0 & 0 & 0 & 0 & 0 \\ 1 & -2 & 0 & 0 & 0 & 0 \\ 1 & 0 & -2 & 0 & 0 & 0 \\ 0 & 1 & 0 & 0 & 0 & 0 \\ 0 & 1 & 1 & 0 & 0 & 0 \\ 0 & 0 & 1 & 0 & 0 & 0 \end{pmatrix}, \quad \mathbf{C}_3 = \begin{pmatrix} 0 & 0 & 0 & 0 & 0 & 0 \\ 0 & 0 & 0 & 0 & 0 & 0 \\ 0 & 0 & 0 & 0 & 0 & 0 \\ 0 & 0 & 0 & -1 & 0 & 0 \\ 0 & 0 & 0 & 0 & -1 & 0 \\ 0 & 0 & 0 & 0 & 0 & -1 \end{pmatrix} \tag{A4}$$

2. Perturbation analysis of the intact-histone, spontaneous detachment model

We will develop a series expansion of the eigenvector $\mathbf{v}_0$ associated with the principal eigenvalue $\lambda_0 \equiv \lambda_0(s)$ of $\mathbf{W}(s) = \mathbf{A} + \varepsilon\mathbf{B} + s\mathbf{C}$ and use it to compute the eigenvalue $\lambda_0(s)$ as a function of s.

We begin with a general observation. Let $\mathbf{H}$ be a matrix with a simple eigenvalue 0. Define $\overline{\mathbf{H}}$ as the submatrix of $\mathbf{H}$ obtained by deleting the first row and column, and assume in addition that $|\overline{\mathbf{H}}| \neq 0$. Denote the first column of $\mathbf{H}$ excluding the first-row element by $\overline{\mathbf{h}}$. If $\mathbf{v}$ is an eigenvector of $\mathbf{H}$ with eigenvalue 0 and is written in the form $\mathbf{v} = \begin{bmatrix} 1 \\ \overline{\mathbf{v}} \end{bmatrix}$, then $\mathbf{H}\mathbf{v} = 0\mathbf{v} = 0$. This implies

$\overline{\mathbf{h}} + \overline{\mathbf{H}}\overline{\mathbf{v}} = 0$ and the general relationship

$$\overline{\mathbf{v}} = -\overline{\mathbf{H}}^{-1}\overline{\mathbf{h}}. \tag{A5}$$

Principal eigenvector for $\mathbf{W}(0)$. Since $\mathbf{W}(0) = \mathbf{A} + \varepsilon\mathbf{B}$ is a transition matrix associated with a reversible Markov chain, the eigenvector associated with the 0-eigenvalue is

$$\mathbf{v}_0(s = 0) = \begin{bmatrix} 1 \\ \varepsilon\mathbf{1}_2 \\ \vdots \\ \varepsilon^{N-1}\mathbf{1}_N \end{bmatrix}, \tag{A6}$$

where $\mathbf{1}_i \in \mathbb{R}^i$ is a vector of all ones.

Series expansion for $\mathbf{v}_0(s)$. Now, we set $\mathbf{H} \equiv \mathbf{W}(s) - \lambda_0(s)\mathbf{I}$, denote the associated principal eigenvector by $\mathbf{v}(s)$, and express it in the form $\mathbf{v}_0(s) = \begin{bmatrix} 1 \\ \overline{\mathbf{v}}_0(s) \end{bmatrix}$. Then, using Eq. (A5),

$$\overline{\mathbf{v}}_0(s) = -\left[\overline{\mathbf{W}}(0) + s\overline{\mathbf{C}} - \lambda_0(s)\mathbf{I}\right]^{-1}\overline{\mathbf{w}} = -\left[\mathbf{I} + s\overline{\mathbf{W}}^{-1}(0)\overline{\mathbf{C}} - \lambda_0(s)\overline{\mathbf{W}}^{-1}(0)\right]^{-1}\overline{\mathbf{W}}^{-1}(0)\overline{\mathbf{w}}, \tag{A7}$$

where $\overline{\mathbf{h}}$ in Eq. (A5) is set to $\overline{\mathbf{w}}$ which is equivalent to the first column of $\mathbf{W}(s)$, minus the first element, and is independent of s. All terms that depend on the perturbation s are explicitly indicated. Recall the Neumann series expansion for $(\mathbf{I} + \mathbf{T})^{-1} = \sum_{k=0}^{\infty}\mathbf{T}^k$ provided the operator norm $\|T\| < 1$. In this case, we can write

$$\overline{\mathbf{v}}_0(s) = -\left[\mathbf{I} + \sum_{k=1}^{\infty}\left(\lambda_0(s)\overline{\mathbf{W}}^{-1}(0) - s\overline{\mathbf{W}}^{-1}(0)\overline{\mathbf{C}}\right)^k\right]\overline{\mathbf{W}}^{-1}(0)\overline{\mathbf{w}}. \tag{A8}$$

Radius of convergence. We first estimate the values of λ and s for which series expansion (A8) converges. This amounts to evaluating the operator norm of the term $(\lambda_0(s)\overline{\mathbf{W}}(0)^{-1} - s\overline{\mathbf{W}}(0)^{-1}\overline{\mathbf{C}})$. Since $\mathbf{C}$ is diagonal with entries 0 and -1, $\|\overline{\mathbf{C}}\| = 1$, and we find the bound

$$\|\lambda_0(s)\overline{\mathbf{W}}^{-1}(0) - \overline{\mathbf{W}}^{-1}(0)s\overline{\mathbf{C}}\| \leq |\lambda_0(s)|\|\overline{\mathbf{W}}^{-1}(0)\| + s\|\overline{\mathbf{W}}^{-1}(0)\|\|\overline{\mathbf{C}}\| \leq \left(|\lambda_0(s)| + s\right)\|\overline{\mathbf{W}}^{-1}(0)\|. \tag{A9}$$

Estimating the operator norm of $\overline{\mathbf{W}}^{-1}(0)$ is more involved. We note that $\hat{\mathbf{Q}}_{1,1}(0)$ is an $N(N+1)/2 - 1 \times N(N+1)/2 - 1$ matrix. An upper bound for the operator norm is given by

$$\|\overline{\mathbf{W}}^{-1}\| \leq \frac{(N+2)(N-1)}{2}\max_{i,j}|\overline{\mathbf{W}}^{-1}(i,j)|. \tag{A10}$$

We now characterize the entries of $\overline{\mathbf{W}}^{-1}(0)$ by applying the same perturbation formula again to $\overline{\mathbf{W}}(0) = \overline{\mathbf{A}} + \varepsilon\overline{\mathbf{B}}$. Note that $\mathbf{A}$ and $\mathbf{B}$ are block tridiagonal and $\mathbf{A}$ is upper-triangular:

$$\overline{\mathbf{W}}(0) = \overline{\mathbf{A}} + \varepsilon\overline{\mathbf{B}} = \begin{bmatrix} \mathbf{D}_1 & \mathbf{F}_2 & \mathbf{0} & \cdots & & \mathbf{0} \\ \mathbf{0} & \mathbf{D}_2 & \mathbf{F}_3 & \ddots & & \vdots \\ \vdots & \ddots & \ddots & \ddots & & \mathbf{0} \\ \vdots & & & \ddots & \ddots & \mathbf{F}_{N-1} \\ \mathbf{0} & \cdots & & \cdots & \mathbf{0} & \mathbf{D}_{N-1} \end{bmatrix} + \varepsilon \begin{bmatrix} \mathbf{D}'_1 & \mathbf{0} & \cdots & & \cdots & \mathbf{0} \\ \mathbf{F}_2^\mathsf{T} & \mathbf{D}'_2 & \ddots & & & \vdots \\ \mathbf{0} & \ddots & \ddots & \ddots & & \vdots \\ \vdots & \ddots & \ddots & \mathbf{D}'_{N-2} & \mathbf{0} \\ \mathbf{0} & \cdots & & \mathbf{0} & \mathbf{F}_{N-1}^\mathsf{T} & \mathbf{0} \end{bmatrix}, \quad \text{(A11)}$$

in view of the block matrix representations given by Eqs (A1) and (A2). Since $\overline{\mathbf{A}}$ is bidiagonal, its inverse is

$$\overline{\mathbf{A}}^{-1} = \begin{bmatrix} \mathbf{D}_1^{-1} & \cdots & \cdots & \cdots & & * \\ \mathbf{0} & \mathbf{D}_2^{-1} & \ddots & \ddots & & \vdots \\ \vdots & & \ddots & \ddots & \ddots & \vdots \\ \vdots & & & \ddots & \ddots & \vdots \\ \mathbf{0} & \cdots & & \cdots & \mathbf{0} & \mathbf{D}_{N-1}^{-1} \end{bmatrix} \quad \text{(A12)}$$

and we can expand the inverse $\overline{\mathbf{W}}^{-1}(0)$ as

$$\overline{\mathbf{W}}^{-1}(0) = \overline{\mathbf{A}}^{-1} + \sum_{i=1}^{\infty} (-\varepsilon\overline{\mathbf{A}}^{-1}\overline{\mathbf{B}})^i \overline{\mathbf{A}}^{-1}$$

$$= \begin{bmatrix} \mathbf{D}_1^{-1} + o(1) & \cdots & & \cdots & \cdots & * \\ O(\varepsilon) & \mathbf{D}_2^{-1} + o(1) & \ddots & & \ddots & \vdots \\ \vdots & & \ddots & & \ddots & \vdots \\ \vdots & & & \ddots & \ddots & \vdots \\ O(\varepsilon^{N-2}) & & \cdots & & \cdots & O(\varepsilon) & \mathbf{D}_{N-1}^{-1} + o(1) \end{bmatrix}$$

$$= \begin{bmatrix} O(1) & \cdots & \cdots & \cdots & O(1) \\ O(\varepsilon) & O(1) & \ddots & \ddots & O(1) \\ \vdots & & \ddots & \ddots & O(1) \\ \vdots & & & \ddots & \ddots & O(1) \\ O(\varepsilon^{N-2}) & \cdots & & \cdots & O(\varepsilon) & O(1) \end{bmatrix}. \quad \text{(A13)}$$

Here, each $*$ denotes a block matrix with entries of order $O(1)$.

We can show by induction that the maximum entry of $\overline{\mathbf{A}}^{-1}$ is less or equal to 1. Therefore, the maximum entry of $\overline{\mathbf{W}}^{-1}$ is bounded by $1 + O(\varepsilon)$ and we conclude that the radius of convergence of the series expansion in Eq. (A8) is

$$s + |\lambda_0(s)| \leq \frac{2}{(N+2)(N-1)(1 + O(\varepsilon))}. \quad \text{(A14)}$$

In other words, the series expansion can be valid even if $s \geq \varepsilon$. The radius of convergence is principally determined by the operator norm of $\overline{\mathbf{A}}^{-1}$.

Perturbations to the eigenvector. We next explicitly evaluate how the eigenvector changes under first order perturbation. Expanding Eq. (A8) to first order in $s + |\lambda|$,

we find

$$\overline{\mathbf{v}}_0(s) = \overline{\mathbf{v}}_0(0) + \overline{\mathbf{W}}^{-1}(0)(\lambda_0(s)\mathbf{I} - s\overline{\mathbf{C}})\overline{\mathbf{v}}_0(0) + O((s + |\lambda|)^2). \quad \text{(A15)}$$

Inserting the estimate of $\overline{\mathbf{W}}^{-1}$ from Eq. (A13), the definition of $\overline{\mathbf{C}}$, and $\mathbf{v}(0)$ derived from Eq. (A6) into Eq. (A15), we observe that

$$\overline{\mathbf{W}}^{-1}(0)\overline{\mathbf{v}}_0(0) = \begin{bmatrix} O(\varepsilon)\mathbf{1}_2 \\ O(\varepsilon^2)\mathbf{1}_3 \\ \vdots \\ O(\varepsilon^{N-1})\mathbf{1}_N \end{bmatrix},$$

$$\overline{\mathbf{W}}^{-1}(0)\overline{\mathbf{C}}\overline{\mathbf{v}}_0(0) = \begin{bmatrix} O(\varepsilon^{N-1})\mathbf{1}_2 \\ O(\varepsilon^{N-1})\mathbf{1}_3 \\ \vdots \\ O(\varepsilon^{N-1})\mathbf{1}_N \end{bmatrix}. \quad \text{(A16)}$$

Let $\mathbf{1}$ be the vector with all entries equal to 1. The eigenvalue $\lambda_0(s)$ satisfies the equation

$$
\begin{aligned}
\lambda_0(s) &= \frac{\mathbf{1}^\mathsf{T}\mathbf{W}(s)\begin{bmatrix} 1 \\ \bar{\mathbf{v}}_0(s) \end{bmatrix}}{\mathbf{1}^\mathsf{T}\bar{\mathbf{v}}_0}(s) \\
&= \frac{\mathbf{1}^\mathsf{T}s\bar{\mathbf{C}}\bar{\mathbf{v}}_0(s)}{\mathbf{1}^\mathsf{T}\bar{\mathbf{v}}_0(s)} \\
&= s\mathbf{1}^\mathsf{T}\bar{\mathbf{C}}\bar{\mathbf{v}}_0(0) + s\mathbf{1}^\mathsf{T}\bar{\mathbf{C}}\bar{\mathbf{W}}^{-1}(0)\bar{\mathbf{v}}_0(0)\lambda_0(s) \\
&\qquad + s^2\mathbf{1}^\mathsf{T}\bar{\mathbf{C}}\bar{\mathbf{W}}^{-1}(0)\bar{\mathbf{C}}\bar{\mathbf{v}}_0(0) \\
&= -Ns\varepsilon^{N-1} + sO(\varepsilon^{N-1})\lambda_0(s) + s^2 O(\varepsilon^{N-1}).
\end{aligned}
\tag{A17}
$$

Therefore, the lowest order approximation to the eigenvalue is

$$
\lambda_0(s) \approx -Ns\varepsilon^{N-1} + O(s^2\varepsilon^{N-1}) = -Ns\varepsilon^{N-1}\big(1 + O(s)\big).
\tag{A18}
$$

This approximation holds whenever $s \ll 1$, (even if $s \gg \varepsilon$), which guarantees the convergence of the series expansion in Eq. (A8).

Substituting Eqs. (A16) and (A18) back into Eq. (A15), we find the lowest order approximation to the eigenvector

$$
\mathbf{v}_0(s) = \begin{bmatrix}
1 \\
\big(\varepsilon + \lambda_0(s)O(\varepsilon) + sO(\varepsilon^{N-1})\big)\mathbf{1}_2 \\
\big(\varepsilon^2 + \lambda_0(s)O(\varepsilon^2) + sO(\varepsilon^{N-1})\big)\mathbf{1}_3 \\
\vdots \\
\big(\varepsilon^{N-1} + \lambda_0(s)O(\varepsilon^{N-1}) + sO(\varepsilon^{N-1})\big)\mathbf{1}_N
\end{bmatrix}.
\tag{A19}
$$

Given that $\lambda_0(s) = O(s\varepsilon^{N-1})$, for each component $v_0(n_1, n_2; s)$ of $\mathbf{v}_0(s)$, we have

$$
v_0(n_1, n_2; s) = \big(1 + O(s)\big)v_0(n_1, n_s; 0).
\tag{A20}
$$

3. Eigenvalues and first passage times

Here, we present some general results on the eigenvalues and eigenvectors of the transition matrix $\mathbf{W}(s)$ and their relation to FPTs.

First, let $\lambda, \mathbf{v}$ be an eigenvalue and eigenvector of $\mathbf{W}(s)$, respectively, such that $\lambda \leq 0$ and all components of $\mathbf{v}$ are nonnegative. Since the probability vector $\mathbf{P}(t)$ satisfies $\mathrm{d}\mathbf{P}/\mathrm{d}t = \mathbf{WP}$, if $\mathbf{P}(0) = \mathbf{v}$, then $\mathbf{P}(t) = e^{\lambda t}\mathbf{v}$.

In a FPT problem, we set the target state Ω^* to be absorbing. Restriction of the transition matrix on states other than Ω^* makes the total probability $P_{\mathrm{tot}}(t) = P[X(t) \notin \Omega^*] = \langle \mathbf{1}, \mathbf{P}(t) \rangle$ nonincreasing with time t, where $X(t)$ is used to denote a random trajectory of the system, and $\langle \cdot, \cdot \rangle$ is the Euclidean inner product, i.e., $\langle \mathbf{x}, \mathbf{y} \rangle = \sum_{(n_1,n_2)\in\Omega} x(n_1, n_2)y(n_1, n_2)$.

In other words, $P_{\mathrm{tot}}(t)$ indicates the probability that the system has not reached the target state Ω^* by time t, and is equivalent to the survival probability in the context of FPT problems. $-\mathrm{d}P_{\mathrm{tot}}/\mathrm{d}t$ is the probability density function of the FPT to Ω^*, and is denoted by $f(t)$.

When $\mathbf{P}(0) = \mathbf{v}$, we have $\mathbf{P}(t) = e^{\lambda t}\mathbf{v}$ and $P_{\mathrm{tot}}(t) = \langle \mathbf{1}, \mathbf{P}(t) \rangle = e^{\lambda t}\langle \mathbf{1}, \mathbf{P}(0) \rangle$. In view of the probabilistic interpretation of $P_{\mathrm{tot}}(t)$, we may assume that $\mathbf{v}$ is normalized, i.e., $\langle \mathbf{1}, \mathbf{v} \rangle = 1$. Therefore, we have

$$
P_{\mathrm{tot}}(t) = e^{\lambda t}, \quad f(t) = -\lambda e^{\lambda t}.
\tag{A21}
$$

Here $f(t)$ represents the distribution of first passage times to Ω^* from a normalized non-negative eigenvector $\mathbf{v}$, and follows an exponential distribution with rate $-\lambda$. The MFPT is thus given by $1/(-\lambda)$.

Next, consider the case where eigenvalues of $\mathbf{W}$ satisfies $0 > \lambda_0 \gg \mathrm{Re}(\lambda_i), \forall i \geq 1$, and the eigenvector $\mathbf{v}_0$ associated with λ_0 is nondegenerate, nonnegative, and normalized. For simplicity, we assume that $\mathbf{W}$ is diagonalizable although this can be relaxed by considering the Jordan canonical form of non-diagonalizable matrices.

Let $\mathbf{P}(0) = \mathbf{P}_0$ be an arbitrary distribution over the states other than Ω^*, then $\mathbf{P}_0$ admits a unique decomposition $\mathbf{P}_0 = \sum_{i=0}^{N-1} c_i\mathbf{v}_i$, where $\mathbf{v}_i$ is the eigenvector of $\mathbf{W}$ associated with λ_i. By linearity of the equation $\mathrm{d}\mathbf{P}/\mathrm{d}t = \mathbf{WP}$, the solution is given by

$$
\mathbf{P}(t) = \sum_{i=0}^{N-1} c_i e^{\lambda_i t}\mathbf{v}_i = e^{\lambda_0 t}\sum_{i=0}^{N(N+1)/2} c_i\mathbf{v}_i e^{(\lambda_i - \lambda_0)t}.
\tag{A22}
$$

When $\mathrm{Re}(\lambda_i) \ll \lambda_0 < 0$, $\mathrm{Re}(\lambda_i - \lambda_0) \ll 0, \forall i \geq 0$ and we have

$$
\begin{aligned}
\mathbf{P}(t) &= c_0 e^{\lambda_0 t}\mathbf{v}_0 + O\left(e^{-\mathrm{Re}(\lambda_1 - \lambda_0)t}\right), \\
P_{\mathrm{tot}}(t) &= c_0 e^{\lambda_0 t} + O\left(e^{-\mathrm{Re}(\lambda_1 - \lambda_0)t}\right).
\end{aligned}
\tag{A23}
$$

That is to say, in the long time limit, the probability distribution of the system is dominated by the eigenvector $\mathbf{v}_0$, and the survival probability $P_{\mathrm{tot}}(t)$ decays exponentially with rate λ_0. The MFPT is thus given by $c_0/(-\lambda_0)$.

This analysis applies to a general FPT problem. In our specific case of nucleosome disassembly and other scenarios where the *absorbing boundary method* is applicable, the transition matrix $\mathbf{W}$ can be considered as a perturbed transition matrix of an irreducible Markov chain. In other words, there exists a decomposition $\mathbf{W} = \mathbf{W}_0 + s\Delta\mathbf{W}$, where s is a small parameter. We treat the eigenvectors and eigenvalues as functions of s, denoted as $\lambda_i(s)$ and $\mathbf{v}_i(s)$, respectively.

Since $\mathbf{W}_0$ is a transition matrix of a continuous time Markov chain, we have $\mathbf{1}^\mathsf{T}\mathbf{W}_0 = \mathbf{0}$, i.e., $\mathbf{1}$ is a left eigenvector of $\mathbf{W}_0$ associated with eigenvalue 0. Therefore, we have

$$
0 = \langle \mathbf{1}, \mathbf{W}_0\mathbf{v}_i(0) \rangle = \lambda_i(0)\langle \mathbf{1}, \mathbf{v}_i(0) \rangle.
\tag{A24}
$$

Irreducibility implies $\lambda_i \neq 0$ for all $i \geq 1$ and thus $\langle \mathbf{1}, \mathbf{v}_i(0) \rangle = 0$ for all $i \geq 1$. Therefore, under small perturbation, we have $\langle \mathbf{1}, \mathbf{v}_i(s) \rangle = \langle \mathbf{1}, \mathbf{v}_i(0) \rangle + O(s)$ as $s \to 0$. We may in addition require that $\langle \mathbf{1}, \mathbf{v}_0(0) \rangle = 1$. Note that $\langle \mathbf{1}, \mathbf{P}_0 \rangle = 1$ for any probability vector $\mathbf{P}_0$. Therefore,

$$
\begin{aligned}
1 &= \langle \mathbf{1}, \mathbf{P}_0 \rangle \\
&= \left\langle \mathbf{1}, \sum_{i \geq 0} c_i \mathbf{v}_i(s) \right\rangle \\
&= c_0 \big[1 + O(s) \big] + \sum_{i \geq 1} c_i O(s) \\
&= c_0 \big[1 + O(s) \big] + O(s)
\end{aligned}
\tag{A25}
$$

and $c_0 \sim 1 + O(s)$. Consequently, in the case of the intact-histone, unfacilitated disassembly model, the MFPT $\mathbb{E}[T(\mathbf{x})]$ from any initial state $\mathbf{x}$ in Ω to the fully detached state Ω^* is given by

$$
\mathbb{E}[T(\mathbf{x})] = \frac{1}{-\lambda_0} + O(s).
\tag{A26}
$$

Moreover, $T(\mathbf{x})$ is approximately exponentially distributed with rate $-\lambda_0$ for any initial state $\mathbf{x}$ in Ω so that

$$
\mathbb{P}(T(\mathbf{x}) \leq t) = 1 - e^{\lambda_0 t} + O(s).
\tag{A27}
$$

The asymptotic exponential distribution and fast relaxation to the steady state properties of this simple system make it possible to treat the simple model as a single coarse-grained state, with transition rates $Ne^{-N\varepsilon}$ to Ω^*.

When other slower transitions are present, we can separate the fast internal relaxation to steady state $\mathbf{v}_0(s)$ and slow dynamics for transitions to external states. The transition rates to external states can be calculated by averaging over the steady state distribution $\mathbf{v}_0(s)$ and provides a good approximation to the full dynamics, as long as the external transition rates are slower than the relaxation rate $-\operatorname{Re}(\lambda_1) \approx 1$ (measured in units of k_{on}). As an example of this fast-slow variable separation, we apply this approach to the coarse-graining of the intact-histone, remodeler-facilitated disassembly model in Fig. 4. This coarse-graining yields matched principal eigenvalues shown in Fig. 5(b).

To formalize the separation of timescales, we consider the following general form of the perturbed dynamics:

$$
\frac{\mathrm{d}\mathbf{P}(t)}{\mathrm{d}t} = (\mathbf{W} + \delta\mathbf{M})\mathbf{P}(t) + \delta\mathbf{m}(t),
\tag{A28}
$$

In Eq. (A28), $\delta \to 0$ and $\mathbf{M}$ is an additional perturbation to the transition matrix $\mathbf{W} = \mathbf{W}_0 + s\Delta\mathbf{W}$. The vector $\delta\mathbf{m}(t)$ is a source term. In the context of coarse-graining of the intact-histone, remodeler-facilitated disassembly model in Fig. 4, we restrict the transition matrix to the microstates within a coarse-grained macrostate. The vector $\mathbf{m}(t)$ represents the transitions from other macrostates to the given macrostate, while $\delta\mathbf{M}$ represents the transitions from the given macrostate to other macrostates, and $\mathbf{W}$ represents the transitions within the given macrostate.

We can still apply the diagonalization technique $\mathbf{W} = \mathbf{V}\mathbf{\Lambda}\mathbf{V}^{-1}$ where $\mathbf{\Lambda}$ is a diagonal matrix with diagonal entries λ_i and $\mathbf{V}$ is a matrix whose columns are the eigenvectors of $\mathbf{W}$.

$$
\frac{\mathrm{d}\mathbf{P}(t)}{\mathrm{d}t} = \mathbf{V}\mathbf{\Lambda} + \delta\mathbf{M}\mathbf{V}[\mathbf{V}^{-1}\mathbf{P}(t)] + \delta\mathbf{m}(t).
\tag{A29}
$$

Left multiply by $\mathbf{1}^{\intercal}$ and recall that as $s \to 0$, $\mathbf{1}^{\intercal}\mathbf{V} = [1, 0, \cdots, 0] + O(s)$ and $\mathbf{V}^{-1}\mathbf{P}(t) = [P_{\mathrm{tot}} + O(s), O(s), \cdots, O(s)]^{\intercal}$ for any nonnegative vector $\mathbf{P}(t)$. This yields

$$
\frac{\mathrm{d}P_{\mathrm{tot}}(t)}{\mathrm{d}t} = (\lambda_0 + \delta\mathbf{1}^{\intercal}\mathbf{M}\mathbf{v}_0)P_{\mathrm{tot}}(t) + \delta\mathbf{1}^{\intercal}\mathbf{m}(t) + O(\delta s)
\tag{A30}
$$

as $s \to 0$. Therefore, the survival probability $P_{\mathrm{tot}}(t)$ corresponding to a coarse-grained macrostate can be approximated by the following processes: the coarse-grained state moving to the absorbing state with rate $-\lambda_0$, moving to other coarse-grained states with rate $-\delta\mathbf{1}^{\intercal}\mathbf{M}\mathbf{v}_0$, and other states contributing to the coarse-grained state with rate $\delta\mathbf{1}^{\intercal}\mathbf{m}(t)$. This approximation holds when s and δ are small enough, compared to 1, i.e. k_{on} in the context of our models. In other words, $-\delta\mathbf{1}^{\intercal}\mathbf{M}\mathbf{v}_0$ is the rate at which the original steady state $\mathbf{v}_0$ leaves the coarse-grained state and goes to other states under perturbation of $\delta\mathbf{M}$, and $\delta\mathbf{1}^{\intercal}\mathbf{m}(t)$ is the rate at which other states contribute to any state inside the coarse-grained state.

As a specific example, in Eq. (C1) or Eq. (4) in the main text, we may write the probability vector $\mathbf{P}$ in block form: $[\mathbf{p}_N, \mathbf{p}_{N-1}, ..., \mathbf{p}_1]^{\intercal}$. Consider $\mathbf{p}_N$ as the coarse-grained state, then $\mathbf{W} = \mathbf{W}_N$, $\mathbf{M} = \mathbf{M}_N$, $\mathbf{m}(t) = \sum_j \frac{p_{\mathrm{d}}}{p_{\mathrm{a}}}\mathbf{G}_{N,j}\mathbf{p}_j(t)$, and $\delta = p_{\mathrm{a}}/k_{\mathrm{on}}$.

Appendix B: Processive motor-assisted histone detachment

Processive motors like DNA helicases slide along the DNA, attacking the nucleosome from only one side of the histone-DNA footprint. In this case, the histone is peeled off from the DNA in a one-sided manner. Analogous to the two-sided peeling model, we can also construct a one-sided peeling model consisting of the attached state space $\Omega = \{(m, n) : m + n \leq N - 1\}$. Here m records the position of motor protein and n records the number of remaining histones.

When the remodeler is absent, the energy landscape of the one-sided peeling model is similar to that of the two-sided peeling model, shown in Fig. 2(b). The main difference lies in the degree of degeneracy of each energy level. The lowest energy level is NE_{c}, corresponding to the unique $n_1 = n_2 = 0$ state in the two-sided peeling model and $n = 0$ state in the one-sided peeling model. For other energy levels $(N - j)E_{\mathrm{c}}$, there are $j + 1$ states

in the two-sided peeling model and only 1 state in the one-sided peeling model.

The contribution of degeneracy to the principal eigenvalue of the two-sided model is the factor N in Eq. (2), which represents N degenerate states at the energy level of E_c. In other words, the associated free energy is given by $E_c + \log N$. By contrast, there is no degeneracy in the one-sided peeling model, and the principal eigenvalue is simply given by

$$\lambda_0(\varepsilon) = -s\varepsilon^{N-1}\big[1 + O(s)\big]. \tag{B1}$$

Estimates of the principal eigenvalue of the two-sided remodeler-assisted peeling model given in Eqs. (6), (8), and (9) are built from the simple estimate Eq. (2) of the spontaneous nucleosome disassembly model. The analogous eigenvalues of the one-sided peeling model are constructed from Eq. (B1) and are

$$\hat{\lambda}_0(E_p > E_c) := -\frac{se^{(N-1)\left(E_c - E_p^-\right)}}{1 + e^{(N-1)\left(E_c - E_p^-\right)}}, \tag{B2}$$

$$\hat{\lambda}_0(E_p \to -\infty) := -\min\left\{se^{(N-1)E_c} + \frac{p_a}{k_{on}}\sum_{j=1}^{N-1}e^{jE_c}, s\right\}, \tag{B3}$$

and

$$\hat{\lambda}_{0,p} := \max\left\{\hat{\lambda}_0(E_p \to -\infty), \hat{\lambda}_0(E_p > E_c)\right\} \tag{B4}$$

These estimates are very close to those of the two-sided peeling model as the entropic contribution $(\log N)$ is negligible compared to the enthalpic contribution (NE_c), especially for strong contacts $E_c \ll -1$.

Appendix C: Transition matrix for intact-histone model with remodeling factors

The linear detachment model is generalized to include remodeling factors that can bind to DNA or contact sites on the partially delaminated histone particle. The total transition matrix that connects states in the space $\Omega_p := \{(m_1, m_2, n_1, n_2) \in \mathbb{N}^4 : m_1 + m_2 + n_1 + n_2 < N\}$ is defined by $\mathbf{W}_{N,p}$, which can be expressed in block form:

$$\mathbf{W}_{N,p} = \begin{bmatrix} \mathbf{W}_{N:1} & \mathbf{0} & \cdots & \cdots & \mathbf{0} \\ \mathbf{0} & \mathbf{W}_{N-1:2} & \ddots & \ddots & \vdots \\ \vdots & \mathbf{0} & \ddots & \ddots & \vdots \\ \vdots & \vdots & \ddots & \ddots & \mathbf{0} \\ \mathbf{0} & \cdots & \cdots & \mathbf{0} & \mathbf{W}_{1:N} \end{bmatrix} + \frac{p_a}{k_{on}}\begin{bmatrix} \mathbf{M}_N & \mathbf{0} & \cdots & \cdots & \mathbf{0} \\ \mathbf{M}_{N-1,N} & \mathbf{M}_{N-1} & \ddots & \ddots & \vdots \\ \vdots & & \ddots & \ddots & \vdots \\ \vdots & & & \ddots & \ddots & \mathbf{0} \\ \mathbf{M}_{1,N} & \cdots & \cdots & \mathbf{M}_{1,2} & \mathbf{0} \end{bmatrix} + \frac{p_d}{k_{on}}\mathbf{G} \tag{C1}$$

Here, $\mathbf{W}_n$ is the $\frac{n(n+1)}{2} \times \frac{n(n+1)}{2}$ matrix as defined in the last subsection, and $\mathbf{W}_{n:m}$ is the $\frac{mn(n+1)}{2} \times \frac{mn(n+1)}{2}$ matrix constructed by placing m $\mathbf{W}_n$ matrices along the diagonal blocks. The matrix $\mathbf{M}_{i,j}$ describes the connectivity of transitions induced by remodeler binding while $\mathbf{G}$ describes connectivity of transitions induced by remodeler unbinding. $\mathbf{M}$ and $\mathbf{G}$ depend on the specific transition mechanism. In the case of processive motor proteins that peel histones from DNA, m_1 and m_2 only increase or decrease by 1 as the motor moves forward or backward by one step. For proteins that directly bind to DNA, m_1 and m_2 can change by larger distances depending on the numbers and positions of the collection of bound proteins. For example, when two DNA-histone contact sites are exposed, the protein can bind to either site, and binding to the more interior site results in m increased by 2. On the other hand, when the protein unbinds, since m only tracks the position of inward-most proteins, the next value of m depends on the position of the second most inward protein.

The construction of $\mathbf{H}_N$ depends on how the states are enumerated. We provide a possible enumeration scheme below.

- For the states (m_1, m_2, n_1, n_2), we first group the states by the value of $m_1 + m_2$ in an ascending order. The first $N(N+1)/2$ entries correspond to the value of $(m_1 + m_2) = 0$, the next block represents entries satisfying $(m_1 + m_2) = 1$, where there are $2 \times (N-1)N/2$ of them, and so on.

- Within each block, we further group the states by the value of m_1 in ascending order, then by values of $n_1 + n_2$, n_1 accordingly in ascending order.

- For fixed (m_1, m_2), note that possible (n_1, n_2) states are grouped in the same order as in the previous non-facilitated model. Therefore, the internal transition matrix restricted to those states can be described by the same $\mathbf{W}_{N-(m_1+m_2)}$.

- To obtain the whole block with $m_1 + m_2$ fixed to a certain value, we just collect the corresponding submatrices $\mathbf{W}_{N-(m_1+m_2)}$ and put them in the diagonal entries, giving rise to the notation $\mathbf{W}_{n:2} = \begin{bmatrix} \mathbf{W}_n & \mathbf{0} \\ \mathbf{0} & \mathbf{W}_n \end{bmatrix}$ and so on.

For transitions represented by $\mathbf{M}$ and $\mathbf{G}$, we have detailed their construction in Eqs. (C2-C4).

1. Examples of $\mathbf{M}$ and $\mathbf{G}$ for motor proteins

Instead of giving the explicit matrix forms of $\mathbf{M}$ and $\mathbf{G}$, we characterize them by considering the transitions of m_1, m_2 allowed in the model, i.e., the positive entries in $\mathbf{M}$ and $\mathbf{G}$. For processive motor proteins, transition of the form $(m_1 \to m_1 + 1)$ is allowed only if $n_1 \geq 1$. The transition matrices are then given by

$$
\begin{aligned}
\mathbf{M}[(m_1 + 1, m_2, n_1 - 1, n_2), (m_1, m_2, n_1, n_2)] &= 1, \quad \forall n_1 \geq 1; \\
\mathbf{M}[(m_1, m_2 + 1, n_1, n_2 - 1), (m_1, m_2, n_1, n_2)] &= 1, \quad \forall n_2 \geq 1; \\
\mathbf{G}[(m_1 - 1, m_2, n_1 + 1, n_2), (m_1, m_2, n_1, n_2)] &= 1, \quad \forall m_1 \geq 1; \\
\mathbf{G}[(m_1, m_2 - 1, n_1, n_2 + 1), (m_1, m_2, n_1, n_2)] &= 1, \quad \forall m_2 \geq 1,
\end{aligned}
\tag{C2}
$$

where $\mathbf{M}[j, i]$ indicates the $i \to j$ transition. The remaining off-diagonal entries in $\mathbf{M}$ and $\mathbf{G}$ are 0. The diagonal entries are determined by the normalization condition that the column sum of $\mathbf{M}$ and $\mathbf{G}$ vanishes from conservation of probability.

One special property of $\mathbf{M}$ and $\mathbf{G}$ for motor proteins is that they are block-tridiagonal matrices. In the block matrix representation shown in Eq. (C1), each block of rows and columns corresponds to a collection of states with the same sum $m_1 + m_2$. For example, $\mathbf{W}_N$ represent transitions within the states with $m_1 + m_2 = 0$ while $\mathbf{M}_{N-1,N}$ represents transitions from the states with $m_1 + m_2 = 0$ to the states with $m_1 + m_2 = 1$.

2. Examples of $\mathbf{M}$ and $\mathbf{G}$ for binding proteins

For proteins that bind to DNA directly, the transitions of the form $(m_1 \to m_1 + k)$ are allowed if $n_1 \geq k$. For the matrix $\mathbf{M}$, we have

$$
\begin{aligned}
\mathbf{M}[(m_1 + k, m_2, n_1 - k, n_2), (m_1, m_2, n_1, n_2)] &= 1, \quad \forall n_1 \geq k; \\
\mathbf{M}[(m_1, m_2 + k, n_1, n_2 - k), (m_1, m_2, n_1, n_2)] &= 1, \quad \forall n_2 \geq k.
\end{aligned}
\tag{C3}
$$

This constraint on n_1 and n_2 arises naturally from the requirement that the target state (m_1', m_2', n_1', n_2') must fall into the state space Ω_p.

For the matrix $\mathbf{G}$, in order to incorporate the different possibilities in the target state when m decreases, we consider two limiting scenarios. In the "high remodeler density" limit, the matrix $\mathbf{G}_{hi}$ is identical to that of the motor proteins, where $m \to m - 1$ when the inner-most remodeler unbinds. In the "low remodeler density" limit, the matrix $\mathbf{G}_{low}$ represents transitions of the form $m \to 0$ since only at most one remodeler is bound per end.

$$
\begin{aligned}
\mathbf{G}_{low}[(0, m_2, n_1 + m_1, n_2), (m_1, m_2, n_1, n_2)] &= 1, \quad \forall m_1 \geq 1; \\
\mathbf{G}_{low}[(m_1, 0, n_1, n_2 + m_2), (m_1, m_2, n_1, n_2)] &= 1, \quad \forall m_2 \geq 1; \\
\mathbf{G}_{hi}[(m_1 - 1, m_2, n_1 + 1, n_2), (m_1, m_2, n_1, n_2)] &= 1, \quad \forall m_1 \geq 1; \\
\mathbf{G}_{hi}[(m_1, m_2 - 1, n_1, n_2 + 1), (m_1, m_2, n_1, n_2)] &= 1, \quad \forall m_2 \geq 1.
\end{aligned}
\tag{C4}
$$

The choices of different $\mathbf{M}$ and $\mathbf{G}$ will not significantly affect the overall histone disassembly rate. For $\mathbf{M}$ associated with remodeler binding and motor proteins, respectively, the effective dissociation rates differ only by $O(\varepsilon)$. Moreover, $\mathbf{G}_{hi}$ and $\mathbf{G}_{low}$ yield qualitatively similar outcomes. When $p_a \lesssim p_d$, the facilitated states are unlikely and do not contribute to the histone unbinding. When $p_a \gg p_d$, unbinding itself is unlikely and their differences are negligible.

3. Irreversible remodeler binding

In this subsection, we assume that $p_{\mathrm{d}} = 0$ and $p_{\mathrm{a}} \ll k_{\mathrm{on}}$. Then, Eq. (C1) becomes

$$\mathbf{W}_{N,\mathrm{p}}(p_{\mathrm{a}}) = \begin{bmatrix} \mathbf{W}_{N:1} + \frac{p_{\mathrm{a}}}{k_{\mathrm{on}}}\mathbf{M}_N & 0 & \cdots & \cdots & 0 \\ \frac{p_{\mathrm{a}}}{k_{\mathrm{on}}}\mathbf{M}_{N-1,N} & \mathbf{W}_{N-1:2} + \frac{p_{\mathrm{a}}}{k_{\mathrm{on}}}\mathbf{M}_{N-1} & \ddots & \ddots & \vdots \\ \vdots & & \ddots & \ddots & \vdots \\ \vdots & & & \ddots & \ddots & 0 \\ \frac{p_{\mathrm{a}}}{k_{\mathrm{on}}}\mathbf{M}_{1,N} & \cdots & & \cdots & \frac{p_{\mathrm{a}}}{k_{\mathrm{on}}}\mathbf{M}_{1,2} & \mathbf{W}_{1:N} \end{bmatrix} \tag{C5}$$

Corresponding to the block matrix representation of $\mathbf{W}_{N,\mathrm{p}}(p_{\mathrm{a}})$ above, we can write the i-th eigenvector $\mathbf{v}_i$ in the form of $\mathbf{v}_i = (\mathbf{v}_{i|N}, \ldots, \mathbf{v}_{i|1})^{\mathsf{T}}$. Here, $\mathbf{v}_{i|N} \in \mathbb{R}^{N(N+1)/2}$ corresponds to the states with $m_1 = m_2 = 0$. If λ is the eigenvalue of this eigenvector, then

$$\lambda(s, p_{\mathrm{a}})\mathbf{v}_{i|N}(s, p_{\mathrm{a}}) = \left(\mathbf{W}_N + \frac{p_{\mathrm{a}}}{k_{\mathrm{on}}}\mathbf{M}_N\right)\mathbf{v}_{i|N}(s, p_{\mathrm{a}}) = \left(\mathbf{W}_N(0) + s\mathbf{C}_N + \frac{p_{\mathrm{a}}}{k_{\mathrm{on}}}\mathbf{M}_N\right)\mathbf{v}_{i|N}(s, p_{\mathrm{a}}), \tag{C6}$$

where we have explicitly indicated the dependency on s and p_{a}. If $\mathbf{v}$ is an eigenvector of $\mathbf{W}_{N,\mathrm{p}}$ with nonvanishing $\mathbf{v}_{i|N}$ terms, then $\mathbf{v}_{i|N}$ is an eigenvector of the matrix $\mathbf{W}_N(s) + p_{\mathrm{a}}/k_{\mathrm{on}}\mathbf{M}_N$. In the following, we will find an estimate for the eigenvalue by using perturbation theory for the matrix $\mathbf{W}_N(s) + p_{\mathrm{a}}/k_{\mathrm{on}}\mathbf{M}_N$ based on the initial state $s = p_{\mathrm{a}} = 0$.

First, we will find a proper initial eigenvector to start the perturbation analysis. When $p_{\mathrm{a}} = 0$, define $\mathbf{v}(s, p_{\mathrm{a}} = 0) = (\mathbf{v}_{i|N}^{\mathsf{T}}(s, 0), 0 \ldots, 0)^{\mathsf{T}}$, where $\mathbf{v}_{i|N}(s, p_{\mathrm{a}} = 0)$ is the principle eigenvector of the matrix $\mathbf{W}_N(s)$ associated with the eigenvalue $Ns\varepsilon^{(N-1)}[1 + O(\varepsilon)]$. Then, $\mathbf{v}(s, 0)$ is an eigenvector of the whole matrix $\mathbf{W}_{N,\mathrm{p}}(p_{\mathrm{a}})$ with eigenvalue 0, for all s.

We next perturb the initial eigenvector $\mathbf{v}_{i|N}(0, 0)$ by applying the same analysis used to obtain Eq. (A8). We find

$$\mathbf{v}_{i|N}(s, p_{\mathrm{a}}, \lambda) = \mathbf{v}_{i|N}(0, 0, 0) + \begin{bmatrix} 0 \\ -\left(\sum_{i=1}^{\infty}\left[-\overline{\mathbf{W}}_N^{-1}(0)(s\bar{\mathbf{C}}_N + p_{\mathrm{a}}/k_{\mathrm{on}}\mathbf{M}_N - \lambda\mathbf{I})\right]^i\right)\bar{\mathbf{v}}_{i|N}(0, 0, 0) \end{bmatrix}, \tag{C7}$$

where λ here is treated as an independent variable. $\bar{\mathbf{v}}_{i|N}(0, 0, 0)$ denotes $\mathbf{v}_{i|N}(0, 0, 0)$ excluding the first row, and $\overline{\mathbf{W}}_N(0)$ is the matrix $\mathbf{W}_N(0) = \mathbf{A}_N + \varepsilon\mathbf{B}_N$ with the first row and column deleted, as defined earlier.

By applying the same estimate over the deviation, we obtain a formula analogous to Eq. (A15),

$$\mathbf{v}_{i|N}(s, p_{\mathrm{a}}, \lambda) = \mathbf{v}_{i|N}(0, 0, 0)\left[1 + O\left(s + |\lambda| + \frac{p_{\mathrm{a}}}{k_{\mathrm{on}}}\right)\right] \tag{C8}$$

and calculate the corresponding eigenvalue by the relation $\lambda = \langle\mathbf{1}, \mathbf{W}\mathbf{v}\rangle/\langle\mathbf{1}, \mathbf{v}\rangle$ for the eigenpair $(\lambda, \mathbf{v})$. In particular, we consider the principal eigenvalue $\lambda_0(s, p_{\mathrm{a}})$ and the corresponding eigenvector $\mathbf{v}_0(s, p_{\mathrm{a}})$ with its first block component $\mathbf{v}_{0|N}$:

$$\begin{aligned} \lambda(s, p_{\mathrm{a}}) &\approx \left\langle\mathbf{1}_{N(N+1)/2}, \left[\mathbf{W}_N(s) + \frac{p_{\mathrm{a}}}{k_{\mathrm{on}}}\mathbf{M}_N\right]\mathbf{x}_N(0, 0)\right\rangle\left[1 + O\left(s + \frac{p_{\mathrm{a}}}{k_{\mathrm{on}}}\right)\right] \\ &\approx -\left(Ns\varepsilon^{N-1} + \frac{p_{\mathrm{a}}}{k_{\mathrm{on}}}\sum_{i=1}^{N-1}(i+1)\varepsilon^i\right)\left[1 + O\left(s + \frac{p_{\mathrm{a}}}{k_{\mathrm{on}}}\right)\right]. \end{aligned} \tag{C9}$$

Eq. (C8) provides a justification for Eq. (7) in the main text, while Eq. (C9) provides a justification for Eq. (8) in the main text.

Determining the eigenvalue when $p_{\mathrm{a}} \gg k_{\mathrm{on}}$ is beyond the scope of this perturbation method because the radius of convergence of the series expansion is around $p_{\mathrm{a}} \sim k_{\mathrm{on}}$. Nonetheless, the simple interpolation formula

$$\lambda(s, p_{\mathrm{a}}) = \max\left\{-\left[Ns\varepsilon^{N-1} + \frac{p_{\mathrm{a}}}{k_{\mathrm{on}}}\sum_{i=1}^{N-1}(i+1)\varepsilon^i\right], -s\right\} \tag{C10}$$

matches numerical calculations quite well when $s = \varepsilon$.

4. Reversible attachment of remodelers

We have not found a succinct analytic description of the predictions of this model; therefore, we adopt a physical approximation by considering the "stability" of $\mathbf{v}_{i|N}$ in order to reduce the block matrix $\mathbf{W}_{N,\mathrm{p}}$ into a $\frac{N(N+1)}{2} \times \frac{N(N+1)}{2}$ matrix connected to (m_1, m_2). The approximation, or coarse-graining, is shown in Fig. 4 and is motivated by a steady state assumption under a fast-slow timescale separation as demonstrated and formalized earlier in Appendix A 3. Assuming that $p_\mathrm{a}, p_\mathrm{d} \ll k_\mathrm{on}$, we note that the relaxation time of states (n_1, n_2) given fixed m_1, m_2 is on the order of k_on. Before any remodeler binding and unbinding transition occurs, it is very likely that the probability distribution of (n_1, n_2) conditioned on (m_1, m_2) has reached a quasi-equilibrium state close to $\mathbf{v}_0$ with $N - m_1 - m_2$ number of contact sites. In such a quasi-equilibrium state, the mean rate of remodeler dissociation will be p_d and the mean rate of another remodeler binding at a distance k position from a free end will be $p_\mathrm{a}\varepsilon^k$ for binding proteins. The overall approximation approach seeks to ignore the fine details of (n_1, n_2) given (m_1, m_2) and approximates the transitions $(m_1, m_2) \to (m_1', m_2')$ as Markovian.

For convenience, we further ignore transitions with rate $p_\mathrm{a}\varepsilon^k$ for $k \geq 2$. This truncation allows for a simple solution for the eigenvector corresponding to the greatest eigenvalue. In the "high remodeler density" limit (stepwise remodeler movement), the simplified transition matrix H_N', defined on $\Omega_\mathrm{p}' := \{(m_1, m_2) : m_1 + m_2 < N\}$, can be expressed as

$$\mathbf{W}_{N,\mathrm{p}}'(p_\mathrm{a}, p_\mathrm{d}) = \mathrm{diag}\{-Ns\varepsilon^{N-1}, -(N-1)s\varepsilon^{N-2}, ..., -s\} + \frac{p_\mathrm{d}}{k_\mathrm{on}}\mathbf{A}_N + \frac{p_\mathrm{a}}{k_\mathrm{on}}\varepsilon\mathbf{B}_N. \tag{C11}$$

The first term describes transitions directly to the detached states Ω_p^* and other terms describes binding and unbinding of a remodeler. Analogy of this simplified scenario to the unfacilitated unbinding model is shown in Fig. 4(a). The approximation showed numerical agreement with the full model in the main text. In the following, we employ additional approximation techniques to derive an analytical expression for the principal eigenvalue when $p_\mathrm{a} + p_\mathrm{d} \gg k_\mathrm{off}$.

We can analytically approximate the principal eigenvalue of $\mathbf{W}_{N,\mathrm{p}}'(p_\mathrm{a}, p_\mathrm{d})$ defined in Eq. (C11) only when $\varepsilon \ll p_\mathrm{a} + p_\mathrm{d}$, where detailed balance approximately holds. In this case, we still assume that the structure $\mathbf{v}_0(m_1, m_2) \propto (\frac{p_\mathrm{a}}{p_\mathrm{d}})^k$ is stable under the small perturbation determined by ε, providing the estimate by considering the normalized flux from the bound states Ω_p' to the fully open states $\Omega_\mathrm{p}'^*$:

$$\begin{aligned}
\lambda_0(p_\mathrm{a}, p_\mathrm{d}, \varepsilon) &\approx \frac{\langle \mathbf{1}_{N(N+1)/2}, (\mathbf{H}'(p_\mathrm{a}, p_\mathrm{d}, 0) - \mathrm{diag}\{Ns\varepsilon^{N-1}, -(N-1)s\varepsilon^{N-2}, ..., s\})\mathbf{v}_0\rangle}{\langle \mathbf{1}_{N(N+1)/2}, \mathbf{v}_0\rangle} \\
&= \varepsilon^N \frac{\sum_{k=0}^{N-1}(k+1)(N-k)K_A^k}{\sum_{k=0}^{N-1}(k+1)(\varepsilon K_A)^k},
\end{aligned} \tag{C12}$$

where, $K_A \equiv \frac{p_\mathrm{a}}{p_\mathrm{d}} = e^{-E_\mathrm{P}}$. Eq. (C12) can be further simplified to Eq. (6) by considering only the first term ($k = 0$) in the numerator, and the first and last term ($k = 0, N-1$) in the denominator.

The coarse-grained approximation of the right-hand side of Eq. (C12) coincides with the prediction via the flux intensity $j(\Omega_\mathrm{p}'^*|\Omega_\mathrm{p}')$. In general, for a continuous time Markov chain with transition rate matrix W, let A and B be two disjoint sets of states, and π be the stationary distribution of the Markov chain. Then the flux intensity from A to B is defined as

$$j(A \mid B) = \frac{\sum_{a \in A} \sum_{b \in B} W_{a,b}\pi_b}{\sum_{b \in B} \pi_b}. \tag{C13}$$

The flux intensity $j(\Omega_\mathrm{p}'^*|\Omega_\mathrm{p}')$ serves as an upper bound for the principal eigenvalue λ_0, *e.g.*, Eq. (3.69) in Aldous and Fill[38].

The intuition for the relation between flux intensity and the eigenvalue is as follows: flux intensity is obtained by assuming that the eigenvector with an absorbing boundary has the same structure as that with a reflecting boundary. In reality, presence of an absorbing boundary will decrease the relative weight of states on the boundary, and thus making the associated eigenvalue smaller than the flux intensity. Note that the flux intensity analysis is similar in both the full facilitated model

and the coarse-grained model, which provides a further justification of the coarse-graining.

Appendix D: Histone detachment with random landscapes

Previously, we have assumed that all 14 contact bonds between the histone core and the DNA are identical with the same binding and unbinding rates k_on and k_off. In re-

ality, these can rates vary depending on local DNA base identity, stiffness and/or spontaneous curvature. It is estimated that the contact free energies vary between 1.5 $k_b T$ and 2 $k_b T$[7,59,60]. To account for this heterogeneity, we conduct numerical experiments that assume homogeneous binding rates but random unbinding rates that correspond to iid binding energies E_c that are drawn from a uniform distribution between $1.5 k_B T$ and $2 k_B T$. In this case, as shown in Fig. 12, the variation does not alter the qualitative behavior of the system. Thus our model is well parameterized by just the mean binding energy E_c.
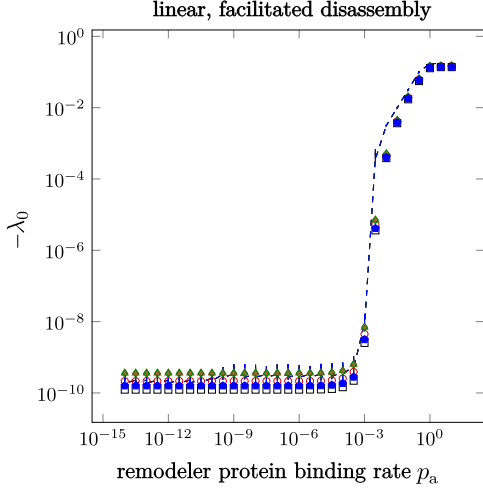
FIG. 12. Principal eigenvalue of the linear facilitated detachment model with random binding energy reflected in variations in k_{off} that lead to a per-site E_c that is uniformly distributed between 1.5 and 2 ($k_B T$). We set $p_d = 10^{-3}$ (in units of k_{on}) and plot $-\lambda_0$ for five randomly sampled configurations of E_c. The dashed line represents the prediction based on mean the binding energy and Eq. (10).

Appendix E: Reversible multimeric histone detachment

Histone dimers, tetramers and other transient higher order complexes in solution may rescue partially disassembled nucleosomes. They can initiate rescue of partially disassembles nucleosomes by directly docking to existing nucleosome subunits (dimers and tetramers) or by associating with the vacant DNA segments. We assume that these rates $q_a'^{(\text{subunit})}$ (for docking with another subunit) and $q_a''^{(\text{subunit})}$ (for direct contact with the DNA) are scaled properly according to their respective equilibrium bulk concentration to ensure that the overall Markov process considering these reactions is *reversible*. We have defined q_a as the docking rate conditioned on both subunits being attached to the DNA.

The primary quantity of interest is the expected time $\mathbb{E}[T(\mathbf{1})]$ needed to transition from the fully attached state $\mathbf{1} = \big(\boldsymbol{\sigma} = (1,1,1,1,1), \mathbf{n} = (0,0)\big) \equiv (1,1,1,1,1,(0,0))$ to the fully dissociated state Ω^*. Solving for the mean detachment time requires inversion of a large matrix over the whole state space, which is analytically intractable. We therefore consider the probability flux intensity $j(\Omega^*|\Omega)$ from the attached states Ω to the fully unattached state Ω^* as a useful surrogate. The general relation between $j(\Omega^*|\Omega)$ and λ_0 is known and derived in *e.g.*, Eq. (3.69) in Aldous and Fill[38], where the inequality $j(\Omega^* | \Omega) \geq |\lambda_0|$ is given.

To obtain a reversible Markov chain, we assume that both bound and free histones are in equilibrium. With our definition of $q_a''^{(\text{subunit})}$, the corresponding free energy relative to bulk solution can be expressed as $\Delta E_s^{(\text{subunit})} = \log\big(k_{on}/q_a''^{(\text{subunit})}\big)$.

The scaling relations between $q_a''^{(\text{subunit})}$ and $q_a'^{(\text{subunit})}$ must follow the equilibrium conditions

$$
\begin{aligned}
q_a'^{(\text{H2A-H2B})} &= q_d^* \exp(-E_q - \Delta E_s^{(\text{H2A-H2B})}), \\
q_a'^{((\text{H3-H4})_2)} &= q_d^* \exp(-E_q - \Delta E_s^{((\text{H3-H4})_2)}), \\
q_a'^{(\text{Hexamer})} &= q_d^* \exp(-2E_q - \Delta E_s^{((\text{H3-H4})_2)} - \Delta E_s^{(\text{H2A-H2B})}), \\
q_a''^{(\text{H2A-H2B})} &= k_{on} \exp(-\Delta E_s^{(\text{H2A-H2B})}), \\
q_a''^{((\text{H3-H4})_2)} &= k_{on} \exp(-\Delta E_s^{((\text{H3-H4})_2)}), \\
q_a''^{(\text{Hexamer})} &= k_{on} \exp(-E_q - \Delta E_s^{(\text{H2A-H2B})} - \Delta E_s^{((\text{H3-H4})_2)}), \\
q_a''^{(\text{Octamer})} &= k_{on} \exp(-2E_q - 2\Delta E_s^{(\text{H2A-H2B})} - \Delta E_s^{((\text{H3-H4})_2)})
\end{aligned}
\tag{E1}
$$

to satisfy reversibility. The free energy function associated with each state $(\boldsymbol{\sigma}, \mathbf{n}) \equiv (\sigma_l, \theta_l, \sigma_m, \theta_r, \sigma_r, \mathbf{n})$ can be expressed as

$$
\begin{aligned}
E(\sigma_l, \theta_l, \sigma_m, \theta_r, \sigma_r, \mathbf{n}) =& (\sigma_l + \sigma_r)\Delta E_s^{(\text{H2A-H2B})} + \sigma_m \Delta E_s^{((\text{H3-H4})_2)} + (\theta_l + \theta_r)E_q \\
& + \Big(N_l \sigma_l + N_m \sigma_m + N_r \sigma_r - \sum_{j=1}^{f}\sum_{k=0}^{1} n_k^{(j)}\Big)E_c.
\end{aligned}
\tag{E2}
$$

In the following, we will further assume $k_{\mathrm{d}} = k_{\mathrm{off}}$, i.e. $s = \varepsilon$, to reduce the notational complexity.

1. Estimate of the flux intensity $j(\Omega^* | \Omega)$ for reversible spontaneous detachment

Let Σ denote the collection of **macrostates** $\boldsymbol{\sigma} = (\sigma_{\mathrm{l}}, \theta_{\mathrm{l}}, \sigma_{\mathrm{m}}, \theta_{\mathrm{r}}, \sigma_{\mathrm{r}})$ that is not equal to $0^{\times 5}$. The microstates on the boundary are characterized by a single intact DNA-histone contact are defined by $\left(N_{\mathrm{l}}\sigma_{\mathrm{l}} + N_{\mathrm{m}}\sigma_{\mathrm{m}} + N_{\mathrm{r}}\sigma_{\mathrm{r}} - \sum_{k,j} n_k^{(j)}\right) = 1$ and denoted by $\partial\Omega$.

The equilibrium flow intensity from bound states that can reach the unbound state in one step can be expressed by enumerating all possible boundary microstates $\mathbf{n}$ associated with each macrostate $\boldsymbol{\sigma}$ in Σ is given by

$$j(\Omega^* | \Omega) = \varepsilon \frac{\sum_{(\boldsymbol{\sigma}, \mathbf{n}) \in \partial\Omega} e^{-E(\boldsymbol{\sigma}, \mathbf{n})}}{\sum_{(\boldsymbol{\sigma}, \mathbf{n}) \in \Omega} e^{-E(\boldsymbol{\sigma}, \mathbf{n})}}, \qquad \text{(E3)}$$

where the free energy can be separated into component energies $E(\boldsymbol{\sigma}, \mathbf{n}) \equiv U(\mathbf{n}) + V(\boldsymbol{\sigma})$ where

$$\begin{aligned}
U(\mathbf{n}) &= -E_{\mathrm{c}} \sum_{j=1}^{f} \sum_{k=0}^{l} n_k^{(j)}, \\
V(\boldsymbol{\sigma}) &= (\sigma_{\mathrm{l}} + \sigma_{\mathrm{r}}) \Delta E_{\mathrm{s}}^{\text{(H2A-H2B)}} + \sigma_{\mathrm{m}} \Delta E_{\mathrm{s}}^{\text{(H3-H4)}_2} \quad \text{(E4)} \\
&\quad + (\theta_{\mathrm{l}} + \theta_{\mathrm{r}}) E_{\mathrm{q}} + N(\boldsymbol{\sigma}) E_{\mathrm{c}}, \\
N(\boldsymbol{\sigma}) &= N_{\mathrm{l}}\sigma_{\mathrm{l}} + N_{\mathrm{m}}\sigma_{\mathrm{m}} + N_{\mathrm{r}}\sigma_{\mathrm{r}},
\end{aligned}$$

where $U(\mathbf{n})$ describes the peeling energy cost of the DNA-histone contacts in the microstate $\mathbf{n}$ and $V(\boldsymbol{\sigma})$ is the energy of the most probable microstate $\mathbf{n}_{\boldsymbol{\sigma}}^*$ given macrostate $\boldsymbol{\sigma}$. $N(\boldsymbol{\sigma})$ is the number of available DNA-histone contacts in macrostate $\boldsymbol{\sigma}$. The denominator in Eq. (E3) is the *partition function* of the equilibrium distribution on Ω.

We can simplify the expression of Eq. (E3) by grouping degenerate states $(\boldsymbol{\sigma}, \mathbf{n}) \in \partial\Omega$ associated with each macrostate $\boldsymbol{\sigma}$ in the numerator and identifying the most probable microstate $\mathbf{n}_{\boldsymbol{\sigma}}^*$ for each macrostate $\boldsymbol{\sigma}$ in the denominator. The most probable microstate $\mathbf{n}_{\boldsymbol{\sigma}}^*$ corresponds to the state with the largest number $N(\boldsymbol{\sigma})$ of DNA-histone contacts. The relative energy of the boundary microstates $\mathbf{n}_{\mathrm{b}}$ compared to the most probable microstate $\mathbf{n}_{\boldsymbol{\sigma}}^*$ for a specified $\boldsymbol{\sigma}$ is $U(\mathbf{n}_{\mathrm{b}}) = -\left[N(\boldsymbol{\sigma}) - 1\right] E_{\mathrm{c}}$. For $\varepsilon = k_{\mathrm{off}}/k_{\mathrm{on}} \ll 1$, $j(\Omega^* | \Omega)$ simplifies to

$$\begin{aligned}
j(\Omega^* | \Omega) &\approx j(E_{\mathrm{c}}) \\
&= \frac{\sum_{\boldsymbol{\sigma} \in S} \varepsilon N(\boldsymbol{\sigma}) e^{-V(\boldsymbol{\sigma}) + E_{\mathrm{c}}[N(\boldsymbol{\sigma}) - 1]}}{\sum_{\boldsymbol{\sigma} \in S} e^{-V(\boldsymbol{\sigma})}}. \quad \text{(E5)} \\
&= \frac{\sum_{\boldsymbol{\sigma} \in S} N(\boldsymbol{\sigma}) e^{-V(\boldsymbol{\sigma}) + E_{\mathrm{c}}[N(\boldsymbol{\sigma})]}}{\sum_{\boldsymbol{\sigma} \in S} e^{-V(\boldsymbol{\sigma})}}
\end{aligned}$$

Note that the exponents in the factor $\sum_{\boldsymbol{\sigma} \in S} e^{-V(\boldsymbol{\sigma})}$ include all possible macrostates, with contributions from both histone-histone interactions (ΔE_{s} and E_{q}) and DNA-histone contacts (E_{c}). Conversely, the exponents in $\sum_{\boldsymbol{\sigma} \in S} N(\boldsymbol{\sigma}) e^{-V(\boldsymbol{\sigma}) + E_{\mathrm{c}}[N(\boldsymbol{\sigma})]}$ take into account only histone-histone interactions.
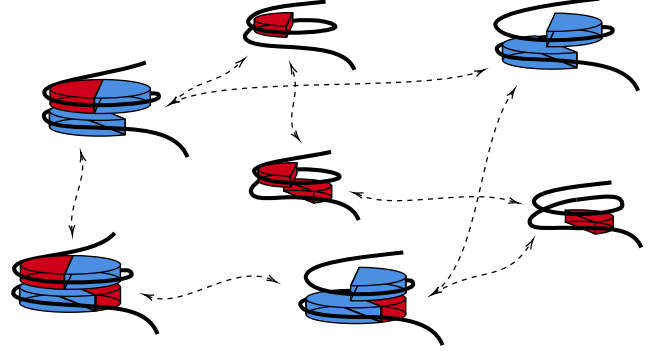
FIG. 13. A schematic of possible macrostates of $(\sigma_{\mathrm{l}}, \sigma_{\mathrm{m}}, \sigma_{\mathrm{r}})$. The states of linkage, $\theta_{\mathrm{l}}, \theta_{\mathrm{r}}$, are omitted for simplicity. For different values of E_{q} and ΔE_{s}, the most probable states are only chosen from either the fully bound state, shown in the lower left corner, or the state where only the (H3-H4)$_2$ tetramer is bound, shown in the upper right corner. Other states are less probable transient states.

We further simplify the formula of $j(\Omega^* | \Omega)$ by considering the relative probability of two main macrostates, the fully bound state $\boldsymbol{\sigma}_1 = (1, 1, 1, 1, 1)$ and the state where only the (H3-H4)$_2$ tetramer is bound $\boldsymbol{\sigma}_{\mathrm{m}} = (0, 0, 1, 0, 0)$. Assuming that $\Delta E_{\mathrm{s}}^{\text{(H3-H4)}_2} = \Delta E_{\mathrm{s}}^{\text{H2A-H2B}}$, the energies of the two macrostates are given by $V(\boldsymbol{\sigma})$:

$$\begin{aligned}
V(\boldsymbol{\sigma}_1) &= 3\Delta E_{\mathrm{s}} + 2E_{\mathrm{q}} + NE_{\mathrm{c}}, \\
V(\boldsymbol{\sigma}_{\mathrm{m}}) &= \Delta E_{\mathrm{s}} + N_{\mathrm{m}}E_{\mathrm{c}}.
\end{aligned} \qquad \text{(E6)}$$

By tracking only these two macrostates, we approximate $j(\Omega^* | \Omega)$ in Eq. (E5) by

$$\begin{aligned}
j(\Omega^* | \Omega) &\approx \frac{N\varepsilon^N e^{-V(\boldsymbol{\sigma}_1)} + N_{\mathrm{m}}\varepsilon^{N_{\mathrm{m}}} e^{-V(\boldsymbol{\sigma}_{\mathrm{m}})}}{e^{-V(\boldsymbol{\sigma}_1)} + e^{-V(\boldsymbol{\sigma}_{\mathrm{m}})}} \\
&= \frac{N\varepsilon^N + N_{\mathrm{m}}\varepsilon^{N_{\mathrm{m}}} e^{\Delta V}}{1 + e^{\Delta V}} \qquad \text{(E7)} \\
&= N\varepsilon^N \frac{1 + (N_{\mathrm{m}}/N) e^{2(E_{\mathrm{q}} + \Delta E_s)}}{1 + e^{\Delta V}},
\end{aligned}$$

where

$$\begin{aligned}
\Delta V &\equiv V(\boldsymbol{\sigma}_1) - V(\boldsymbol{\sigma}_{\mathrm{m}}) \\
&= 2\Delta E_{\mathrm{s}} + 2E_{\mathrm{q}} + (N - N_{\mathrm{m}})E_{\mathrm{c}}.
\end{aligned} \qquad \text{(E8)}$$

Given the discussion of irreversible nucleosome disassembly in the main text, here, we focus on understanding the role of q_{d}^* in nucleosome disassembly and how ΔE_{s} affects reversible histone rebinding. Eq. (E7) explicitly shows the roles of ΔE_{s} and E_{q} in the reversible multimeric nucleosome disassembly.

Irreversible subunit unbinding arises when $\Delta E_{\mathrm{s}} \to \infty$ which is equivalent to $q_{\mathrm{a}}', q_{\mathrm{a}}'' = 0$. In this limit, the

most probable state is the $(H3\text{-}H4)_2$-bound state, with $j(\Omega^*|\Omega) \sim N_m e^{N_m E_c}$. The transition point between an effectively irreversible scenario and a reversible unbinding scenario is when $\Delta V \approx 0$, above which the fully bound macrostate $\boldsymbol{\sigma}_1$ is no longer the most probable state. This transition point is characterized by $(E_q + \Delta E_s) = (N_M - N)E_c/2$.

When ΔE_s is small but still positive, and $\Delta E_s + E_q > 0$, the most probable state is the fully bound state with N DNA-histone contacts. However, the boundary states can be stabilized by absence of one or more histone modules, with $j(\Omega^*|\Omega) \sim N_m e^{N E_c + 2(\Delta E_s + E_q)}$. However, when ΔE_s is negative, absence of one or more histone subunits cannot stabilize the boundary states. In this case, $j(\Omega^*|\Omega) \sim N e^{N E_c}$, which is close to the linear intact histone model.

In the context of a FPT problem from the fully attached state $\boldsymbol{1} = (\boldsymbol{\sigma}_1, \mathbf{n} = (0,0))$ where N histone-DNA contacts must be dissociated to be reach Ω^*, which we formally treat as an absorbing state while still allowing for partial rebinding. The flux intensity $j(\Omega^*|\Omega)$ serves as an estimate of $-\lambda_0$, the principal eigenvalue of the transition matrix with absorbing state Ω^*, which in turn is inversely related to the MFPT $\mathbb{E}[T(\boldsymbol{1})]$. Thus, Eq. (E5) captures the dependence of $\mathbb{E}[T(\boldsymbol{1})]$ on ΔE_s.

We can provide a better estimate of the principal eigenvalue λ_0 of the detachment process under partial histone rebinding by incorporating the rate-limiting effects of the unlinking step into the flux intensity $j(\Omega^*|\Omega)$ and the contribution from the monomeric pathway $N e^{N E_c}$:

$$\hat{\lambda}_{0,q}(E_c, q_d^*) = -\min\left\{ (q_d^*/k_{on} \vee N e^{N E_c}), j(\Omega^*|\Omega) \right\}, \tag{E9}$$

where $(q_d^*/k_{on} \vee N e^{N E_c}) := \max\{q_d^*/k_{on}, N e^{N E_c}\}$. The results of numerical calculations of $\mathbb{E}[T(\boldsymbol{1})]$ and its comparison to $-\lambda_0$ in the irreversible case, as well as the estimates in Eq. (E9) are shown in Fig. 8(b-c). Good agreement between Eq. (E9) and numerical results is observed.

2. Limits of remodeler facilitation

We now consider the case where the disassembly of nucleosomes is facilitated by additional nucleosome remodelers. We make the following observations in different limits of the remodeler strength. These observations parallel the corresponding limits in the linear peeling intact-histone model.

When the binding energy E_p of the remodeler to DNA is strongly negative, and the binding rate $p_a > N_l k_{on} e^{N_l E_c}$, after the dissociation of the histone modules, the remodeler will bind to the DNA and prevent the reassociation of the histone modules. Consequently, the scenario is equivalent to the irreversible, facilitated disassembly of nucleosomes as discussed in the main text, where we have the estimate through Eq. (16) which defines $\mathbb{E}[T]$:

$$-\hat{\lambda}_{0,p,q}(E_p \to -\infty) = -\hat{\lambda}_0(E_p \to -\infty) + \frac{1}{\mathbb{E}[T] + \frac{k_{on}}{q_d^*}} \tag{E10}$$

When the binding energy E_p of the remodeler to DNA is weakly negative, and the binding rate p_a is fast enough, the remodeler effects are limited to modifying the effective contact energy between the histone and DNA in Eq. (E9).

$$\hat{\lambda}_{0,p,q}(E_p > E_c) = \hat{\lambda}_{0,q}(E_c - E_p^-, q_d^*), \tag{E11}$$

where $E_p^- := \min\{E_p, 0\}$. A general estimate of the disassembly rate can be obtained by taking the minimum of the two limits, in terms of absolute values, i.e.,

$$\hat{\lambda}_{0,p,q} := \max\left\{ \lambda_{0,p,q}(E_p > E_c), \hat{\lambda}_{0,p,q}(E_p \to -\infty) \right\}. \tag{E12}$$

The results of this estimate are shown in Fig. 10(b). In slow remodeler binding rate p_a limit, the estimate in Eq. (E12) provides a good approximation to the numerical results. In large p_a regime, the most probable state on Ω switches to the state on the boundary $\partial\Omega$. Thus, λ_0 should be rate-limited by the DNA-histone unbinding rate k_{off} from the boundary state to Ω^*, while the first passage time $\mathbb{E}[T(\boldsymbol{1})]$ starting from the most interior state, $\boldsymbol{1} = (1,1,1,1,1,(0,0))$, is approximately N/k_{off}.

Appendix F: Quantifying contributions from the monomeric and multimeric pathways

We adapt the facilitated, multimeric model to quantify the relative contributions of the monomeric and multimeric disassembly pathways. In the original model, the histone can leave the DNA either as an intact octamer or by disassembling into dimers and tetramers. For example, in the high free histone concentration limit ($\Delta E_s \lesssim 0$) and low remodeler binding rate limit ($p_a \to 0$), as is shown in Fig. 10(b), the histone is prevented from breaking apart since any partial loss of histone modules will be immediately replaced by free histone modules. In this limit, the histone can leave the DNA only as an intact octamer with the slow rate $-\lambda_0 \approx N e^{N E_c}$ associated with the unfacilitated simple intact-histone model given by Eq. (2).

There are different ways to quantify the relative contributions of the different disassembly pathways. One possibility is to evaluate the flux contribution of the monomeric pathway to the total flux associated with the principal eigenvector of the transition matrix. However, in the strong facilitation limit, the principal eigenvector differs significantly from the fully attached state from which we wish to quantify the probability flux. To overcome this discrepancy, we adopt an alternative approach in the FPT formalism. Suppose we start with the state

$\mathbf{1} = (1, 1, 1, 1, 1, (0, 0))$, and split the target state Ω^* into two parts: $\Omega^* = \Omega_1^* \cup \Omega_2^*$.

We define the FPT to Ω_1^* and Ω_2^* as T_1 and T_2, respectively. The original first passage time to Ω^* is thus $T = \min\{T_1, T_2\}$. Transitions into Ω_1^* define histones that leave as an intact octamer, *i.e.*, $\Omega_1^* = \{(1, 1, 1, 1, 1, (n_1 + n_2 = N))\}$. The relative contribution of the pathway that leads to Ω_1^* can be quantified by the probability $\mathbb{P}[T_1 < T_2]$ that $T_1 < T_2$. To compute $\mathbb{P}[T_1(\mathbf{1}) < T_2(\mathbf{1})]$, we employ the standard approach of first passage time formalism. For completeness, we briefly describe the general method below where the symbols used do not necessarily correspond to those previously used.

Consider a continuous-time Markov chain with a discrete state space Ω and the transition matrix $\mathbf{W}$ defined by $\frac{d}{dt}\mathbf{x} = \mathbf{W}\mathbf{x}$. Let $A, B \subseteq \Omega$ and T be the FPT to $A \cup B$. We then find $\mathbb{P}(x_T \in A \,|\, x_0 = x) \equiv P_A(x)$.

We first discretize the Markov chain $\{x_t : t \in \mathbb{R}^+\}$ into a sequence of states $\{x_{t_i} : t_i \in \mathbb{R}^+\}$, where t_i is the i-th time point at which the i-th jump occurs. The sequence $\{x_{t_i} \equiv x_i : i \geq 0\}$ is a discrete-time Markov chain, with the transition probability given by

$$\mathbb{P}(x_{i+1} = y \mid x_i = x) = \frac{W_{y,x}}{-W_{x,x}}.$$

Conditioning on the first jump time t_1, we derive the recursion relation for $P_A(x)$:

$$\begin{aligned}
&\mathbb{P}\left(x_T \in A \,|\, x_0 = x\right) \\
&= \sum_y \mathbb{P}\left(x_T \in A \,|\, x_0 = x, x_1 = y\right) \mathbb{P}\left(x_1 = y \,|\, x_0 = x\right) \\
&= \sum_y \mathbb{P}\left(x_T \in A \,|\, x_0 = y\right) \mathbb{P}\left(x_1 = y \,|\, x_0 = x\right) \\
&= \sum_y P_A(y)\mathbb{P}(y \,|\, x).
\end{aligned}$$

Rearranging, we find

$$W_{x,x}P_A(x) + \sum_{y \neq x} P_A(y)W_{y,x} = 0.$$

$$\mathbf{P}_A^\intercal \mathbf{W} = 0,$$

which can be solved with boundary condition

$$P_A(x) = \begin{cases} 1 & x \in A, \\ 0 & x \in B. \end{cases}$$

In order to more efficiently solve the problem, it is helpful to decompose $\mathbf{W}$ and P_A according to the decomposition of the state space $\Omega = \Omega_* \cup A \cup B$, where A, B, and Ω_* are disjoint. We represent $\mathbf{W}$ by

$$\mathbf{W} = \begin{bmatrix} \mathbf{W}_{\Omega_*,\Omega_*} & \mathbf{W}_{\Omega_*,A} & \mathbf{W}_{\Omega_*,B} \\ \mathbf{W}_{A,\Omega_*} & \mathbf{W}_{A,A} & \mathbf{W}_{A,B} \\ \mathbf{W}_{B,\Omega*} & \mathbf{W}_{B,A} & \mathbf{W}_{B,B} \end{bmatrix}$$

and $\mathbf{P}_A^\intercal$ by

$$\mathbf{P}_A^\intercal = \begin{bmatrix} \mathbf{P}_{A|\Omega_*}^\intercal & \mathbf{P}_{A|A}^\intercal & \mathbf{P}_{A|B}^\intercal \end{bmatrix} = \begin{bmatrix} \mathbf{P}_{A|\Omega*}^\intercal & \mathbf{1}^\intercal & \mathbf{0}^\intercal \end{bmatrix},$$

where the second equality arises from the boundary condition. Solving for $\mathbf{P}_{A|\Omega_*}^\intercal$, we find

$$\mathbf{P}_{A|\Omega_*}^\intercal \mathbf{W}_{\Omega_*,\Omega_*} + \mathbf{1}^\intercal \mathbf{W}_{A,\Omega_*} = \mathbf{0}$$

$$\mathbf{P}_{A|\Omega_*} = -\left(\mathbf{W}_{\Omega_*,\Omega_*}\right)^{-\intercal} \mathbf{W}_{A,\Omega_*}^\intercal \mathbf{1}$$

The numerical solution is shown in Fig. 11. In the limit $p_a \to 0$, the multimeric pathway is typically faster than the monomeric pathway, leading to a smaller probability of the histone leaving as an intact octamer. When $p_a \to \infty$, the multimeric pathway is rate-limited by the histone-module dissociation rate q_d^*, while both pathways are also limited by the histone-DNA dissociation rate k_{off}. When $q_d^* \ll k_{off}$, the monomeric pathway is faster than the multimeric pathway, and the probability of the histone leaving as an intact octamer is close to 1. If $q_d^* \gg k_{off}$ and $p_a \to \infty$, the multimeric pathway and the monomeric pathway carry similar rates and the probability of the histone leaving as an intact octamer is close to $1/2$, as shown in Fig. 11(b).

REFERENCES

[1] H. Schiessel, J. Widom, R. F. Bruinsma, and W. M. Gelbart. Polymer reptation and nucleosome repositioning. *Phys. Rev. Lett.*, 86:4414–4417, 2001.

[2] K. Luger, A. W. Mader, R. K. Richmond, DF Sargent, and T. J. Richmond. Crystal structure of the nucleosome core particle at 2.8 a resolution. *Nature*, 389(6648):251–260, 1997.

[3] Y. Lorch, J. W. Lapointe, and R. D. Kornberg. Nucleosomes inhibit the initiation of transcription but allow chain elongation with the displacement of histones. *Cell*, 49(2):203–210, 1987.

[4] Timothy J. Richmond and Curt A. Davey. The structure of DNA in the nucleosome core. *Nature*, 423(6936):145, 2003.

[5] C. M. Nolan E. R. Gibney. Epigenetics and gene expression. *Heredity*, 105(1):4–13, 2010.

[6] Christopher W. Akey and Karolin Luger. Histone chaperones and nucleosome assembly. *Current Opinion in Structural Biology*, 13(1):6–14, 2003.

[7] J. D. Anderson and J. Widom. Sequence and position-dependence of the equilibrium accessibility of nucleosomal DNA target sites. *Journal of Molecular Biology*, 296(4):979–987, 2000.

[8] Gu Li, Marcia Levitus, Carlos Bustamante, and Jonathan Widom. Rapid spontaneous accessibility of nucleosomal DNA. *Nature Structural & Molecular Biology*, 12(1):46, 2005.

[9] M. Tomschik, H. Zheng, K. V. Holde, J. Zlatanova, and S. H. Leuba. Fast, long-range, reversible conformational fluctuations in nucleosomes revealed by single-pair fluorescence resonance energy transfer. *Proceedings of the National Academy of Sciences of the United States of America*, 102(9):3278–3283, 2005.

[10] Robert A. Forties, Justin A. North, Sarah Javaid, Omar P. Tabbaa, Richard Fishel, Michael G. Poirier, and Ralf Bundschuh. A quantitative model of nucleosome dynamics. *Nucleic Acids Research*, 39:8306–8313, 2011.

[11] Lennart de Bruin, Marco Tompitak, Behrouz Eslami-Mossallam, and Helmut Schiessel. Why do nucleosomes unwrap asymmetrically? *The Journal of Physical Chemistry B*, 120(26):5855–5863, 2016. PMID: 26991771.

[12] M. Tompitak, L. de Bruin, B. Eslami-Mossallam, and H. Schiessel. Designing nucleosomal force sensors. *Phys. Rev. E*, 95:052402, 2017.

[13] Marco Tompitak, Cédric Vaillant, and Helmut Schiessel. Genomes of multicellular organisms have evolved to attract nucleosomes to promoter regions. *Biophysical Journal*, 112(3):505–511, 2017.

[14] J. Culkin, L. de Bruin, M. Tompitak, R. Phillips, and H. Schiessel. The role of DNA sequence in nucleosome breathing. *European Physical Journal E*, 40(11), 2017.

[15] Koen van Deelen, Helmut Schiessel, and Lennart de Bruin. Ensembles of breathing nucleosomes: A computational study. *Biophysical Journal*, 118(9):2297–2308, 2020.

[16] Alexey Shvets, Maria Kochugaeva, and Anatoly Kolomeisky. Mechanisms of protein search for targets on DNA: Theoretical insights. *Molecules*, 23(9):2106, 2018.

[17] Junji Iwahara and Anatoly B. Kolomeisky. Discrete-state stochastic kinetic models for target DNA search by proteins: Theory and experimental applications. *Biophysical Chemistry*, 269:106521, 2021.

[18] Anupam Mondal, Sujeet Kumar Mishra, and Arnab Bhattacherjee. Nucleosome breathing facilitates cooperative binding of pluripotency factors Sox2 and Oct4 to DNA. *Biophysical Journal*, 121(23):4526–4542, 2022.

[19] Anupam Mondal, Cayke Felipe, and Anatoly B. Kolomeisky. Nucleosome breathing facilitates the search for hidden DNA sites by pioneer transcription factors. *The Journal of Physical Chemistry Letters*, pages 4096–4103, 2023.

[20] B. Zhang, W. Zheng, G. A. Papoian, and P. G. Wolynes. Exploring the free energy landscape of nucleosomes. *Journal of the American Chemical Society*, 138(26):8126–8133, 2016.

[21] J. Lequieu, A. Cordoba, D. C. Schwartz, and J. De Pablo. Tension-dependent free energies of nucleosome unwrapping. *Acs Central Science*, 2(9):660, 2016.

[22] David, Winogradoff, Aleksei, and Aksimentiev. Molecular mechanism of spontaneous nucleosome unraveling. *Journal of Molecular Biology*, 2018.

[23] Giovanni B. Brandani, Cheng Tan, and Shoji Takada. The kinetic landscape of nucleosome assembly: A coarse-grained molecular dynamics study. *PLoS Computational Biology*, 17(7):e1009253, 2021.

[24] Tom Chou. Peeling and sliding in nucleosome repositioning. *Phys. Rev. Lett.*, 99:058105, 2007.

[25] Jinsu Kim, Katherine M. Sheu, Quen J. Cheng, Alexander Hoffmann, and German Enciso. Stochastic models of nucleosome dynamics reveal regulatory rules of stimulus-induced epigenome remodeling. *Cell Reports*, 40(2):111076, 2022.

[26] Denis Tolkunov, Karl A. Zawadzki, Cara Singer, Nils Elfving, Alexandre V. Morozov, and James R. Broach. Chromatin remodelers clear nucleosomes from intrinsically unfavorable sites to establish nucleosome-depleted regions at promoters. *Molecular Biology of the Cell*, 22(12):2106–2118, 2011.

[27] P. T. Lowary and J. Widom. Nucleosome packaging and nucleosome positioning of genomic DNA. *Proceedings of the National Academy of Sciences*, 94(4):1183–1188, 1997.

[28] P. T. Lowary and J. Widom. New DNA sequence rules for high affinity binding to histone octamer and sequence-directed nucleosome positioning. *Journal of Molecular Biology*, 276(1):19–42, 1998.

[29] Sture Nordholm. The absorbing boundary method. II. generalization of the golden rule. *The Journal of Chemical Physics*, 71(5):2313, 1979.

[30] Dmitry V. Fyodorov and James T. Kadonaga. Dynamics of ATP-dependent chromatin assembly by ACF. *Nature*, 418(6900):896–900, 2002.

[31] Patrick D Varga-Weisz and Peter B Becker. Regulation of higher-order chromatin structures by nucleosome-remodelling factors. *Current Opinion in Genetics & Development*, 16(2):151–156, 2006.

[32] Kangjing Chen, Junjie Yuan, Youyang Sia, and Zhucheng Chen. Mechanism of action of the SWI/SNF family complexes. *Nucleus*, 14(1), 2023.

[33] Tinka V. M. Clement, Dian Spakman, Andreas S. Biebricher, Graeme A. King, Manika I. Singh, Ian D. Hickson, Erwin J. G. Peterman, and Gijs J. L. Wuite. Pitch-induced nucleosome remodeling studied by dual-trap optical tweezers. *Biophysical Journal*, 121(3):22a–23a, 2022.

[34] Kristina Makasheva, Louise Bryan, Martin Jinek, and Beat Fierz. Multiplexed single-molecule experiments reveal Cas9 nucleosome invasion dynamics. *Biophysical Journal*, 121(3):159a–160a, 2022.

[35] Micah McCauley, Joha Joshi, Michael Morse, Nicole A. Becker, Qi Hu, Zelin Shan, Molly H. Nelson Holte, Uma Muthurajan, Ioulia F. Rouzina, Karolin Luger, Dmitry Lyumkis, Georges Mer, L. James Maher, and Mark C. Williams. Nucleosome chaperones facilitate both nucleosome assembly and disassembly. *Biophysical Journal*, 121(3):3a, 2022.

[36] Bernard Prum and Jean Claude Fort. *Stochastic processes on a lattice and Gibbs measures*, volume 11. Springer Science & Business Media, 1990.

[37] Jeff Bezanson, Alan Edelman, Stefan Karpinski, and Viral B. Shah. Julia: A fresh approach to numerical computing. *SIAM Review*, 59(1):65–98, 2017.

[38] David Aldous and James Allen Fill. *Reversible Markov Chains and Random Walks on Graphs*. unpublished monograph, 2002.

[39] J. O. Thomas and R. D. Kornberg. An octamer of histones in chromatin and free in solution. *Proceedings of the National Academy of Sciences*, 72(7):2626–2630, 1975.

[40] Ahmad Elbahnsi, Romain Retureau, Marc Baaden, Brigitte Hartmann, and Christophe Oguey. Holding the nucleosome together: A quantitative description of the DNA-histone interface in solution. *Journal of chemical theory and computation*, 14(2):1045–1058, 2018.

[41] S. N. Khrapunov, A. I. Dragan, A. V. Sivolob, and A. M. Zagariya. Mechanisms of stabilizing nucleosome structure. Study of dissociation of histone octamer from DNA. *Biochimica et Biophysica Acta (BBA) - Gene Structure and Expression*, 1351(1):213–222, 1997.

[42] Duane A. Hoch, Jessica J. Stratton, and Lisa M. Gloss. Protein–protein Förster Resonance Energy Transfer analysis of nucleosome core particles containing H2A and H2A.Z. *Journal of Molecular Biology*, 371(4):971–988, 2007.

[43] Alexander Gansen, Alessandro Valeri, Florian Hauger, Suren Felekyan, Stanislav Kalinin, Katalin Tóth, Jörg Langowski, and Claus A. M. Seidel. Nucleosome disassembly intermediates characterized by single-molecule FRET. *Proceedings of the National Academy of Sciences of the United States of America*, 106(36):15308–15313, 2009.

[44] Vera Böhm, Aaron Hieb, Andrew Andrews, Alexander Gansen, Andrea Rocker, Katalin Tóth, Karolin Luger, and Jörg Langowski. Nucleosome accessibility governed by the dimer/tetramer interface. *Nucleic acids research*, 39:3093–3102, 2010.

[45] Hiroaki Tachiwana, Wataru Kagawa, Akihisa Osakabe, Koichiro Kawaguchi, Tatsuya Shiga, Yoko Hayashi-Takanaka, Hiroshi Kimura, and Hitoshi Kurumizaka. Structural basis of instability of the nucleosome containing a testis-specific histone variant, human h3t. *Proceedings of the National Academy of Sciences*, 107(23):10454–10459, 2010.

[46] W. E. Arnoldi. The principle of minimized iterations in the solution of the matrix eigenvalue problem. *Quarterly of Applied Mathematics*, 9(1):17–29, 1951.

[47] T. Chou and M. R. D'Orsogna. *First Passage Problems in Biology*, chapter Chapter 13, pages 306–345. World Scientific, 2014.

[48] Ran Chen and Marc S. Wold. Replication protein a: Single-stranded DNA's first responder. *BioEssays*, 36(12):1156–1161, 2014.

[49] Bryan Gibb, Ling F. Ye, Stephanie C. Gergoudis, YoungHo Kwon, Hengyao Niu, Patrick Sung, and Eric C. Greene. Concentration-dependent exchange of replication protein a on single-stranded DNA revealed by single-molecule imaging. *PLoS ONE*, 9(2):e87922, 2014.

[50] M. Nabuan Naufer, Michael Morse, Guðfríður Björg Möller, James McIsaac, Ioulia Rouzina, Penny J. Beuning, and Mark C. Williams. Multiprotein E. coli SSB–ssDNA complex shows both stable binding and rapid dissociation due to interprotein interactions. *Nucleic Acids Research*, 49(3):1532–1549, 2021.

[51] Yasuhiro Arimura, Masae Ikura, Risa Fujita, Mamiko Noda, Wataru Kobayashi, Naoki Horikoshi, Jiying Sun, Lin Shi, Masayuki Kusakabe, Masahiko Harata, Yasuyuki Ohkawa, Satoshi Tashiro, Hiroshi Kimura, Tsuyoshi Ikura, and Hitoshi Kurumizaka. Cancer-associated mutations of histones H2B, H3.1 and H2A.Z.1 affect the structure and stability of the nucleosome. *Nucleic Acids Research*, 46(19):10007–10018, 2018.

[52] D. T. Gruszka, S. Xie, H. Kimura, and H. Yardimci. Single-molecule imaging reveals control of parental histone recycling by free histones during DNA replication. *Science Advances*, 6(38), 2020.

[53] Chou, Tom. An exact theory of histone-DNA adsorption and wrapping. *Europhys. Lett.*, 62(5):753–759, 2003.

[54] Jyotsana J. Parmar, John F. Marko, and Ranjith Padinhateeri. Nucleosome positioning and kinetics near transcription-start-site barriers are controlled by interplay between active remodeling and dna sequence. *Nucleic Acids Research*, 42:128–136, 2013.

[55] Hongyu Zhao, Mingxin Guo, Fenghui Zhang, Xueqin Shao, Guoqing Liu, Yongqiang Xing, Xiujuan Zhao, Liaofu Luo, and Lu Cai. Nucleosome assembly and disassembly in vitro are governed by chemical kinetic principles. *Frontiers in Cell and Developmental Biology*, 9, 2021.

[56] Răzvan V. Chereji, Denis Tolkunov, George Locke, and Alexandre V. Morozov. Statistical mechanics of nucleosome ordering by chromatin-structure-induced two-body interactions. *Phys. Rev. E*, 83:050903, 2011.

[57] Céline Duc and Christophe Thiriet. Replication-coupled chromatin remodeling: An overview of disassembly and assembly of chromatin during replication. *International Journal of Molecular Sciences*, 22(3):1113, 2021.

[58] Wei Zhao, Lingxia Qiao, Shiyu Yan, Qing Nie, and Lei Zhang. Mathematical modeling of histone modifications reveals the formation mechanism and function of bivalent chromatin. *iScience*, 24:102732, 2021.

[59] K.J. Polach and J. Widom. Mechanism of protein access to specific DNA sequences in chromatin: A dynamic equilibrium model for gene regulation. *Journal of Molecular Biology*, 254(2):130–149, 1995.

[60] Igor M. Kulić and Helmut Schiessel. Opening and closing DNA: Theories on the nucleosome. In *DNA Interactions with Polymers and Surfactants*, pages 173–208. John Wiley & Sons, Inc., 2007.